We are IntechOpen, the world's leading publisher of Open Access books Built by scientists, for scientists

4,800
Open access books available

122,000
International authors and editors

135M
Downloads

Our authors are among the

154
Countries delivered to

TOP 1%
most cited scientists

12.2%
Contributors from top 500 universities

CLARIVATE ANALYTICS BOOK CITATION INDEX INDEXED

WEB OF SCIENCE™

Selection of our books indexed in the Book Citation Index in Web of Science™ Core Collection (BKCI)

Interested in publishing with us?
Contact book.department@intechopen.com

Numbers displayed above are based on latest data collected.
For more information visit www.intechopen.com

10

Electromagnetic Response and Broadband Utilities of Planar Metamaterials

Hongqiang Li and Zeyong Wei
Physics Department, Tongji University
China

1. Introduction

Metamaterial (Smith, Pendry et al. 2004) interacts with electromagnetic waves in a resonant manner, affording us new giving rise to a new route for subwavelength photonic devices, such as compact antenna substrate (Li, Hang et al. 2005) and subwavelength resonant cavity (Zhou, Li et al. 2005; Li, Hao et al. 2006). Planar-type configuration,thanks to layer-by-layer fabrication technique, has been recognized as the most efficient and easiest way for the realization of metamaterials from microwave, terahertz, and optical regimes. And it is interesting to note that, in contrast to the common notion that the operational bandwidth of metamaterial is usually very narrow due to the local resonance nature, our recent studies show that planar metamaterial can be broadband in functionality (Wei, Cao et al. 2010; Wei, Cao et al. 2011).

It is worth noting that the studies on plasmonics and metamaterials are heuristic and beneficial to each other. Surface plasmon polaritons (SPPs) modulate light waves at the metal-dielectric interface with wavelength much smaller than that in free space (Raether 1988),which enables the control of light in a subwavelength scale for nanophotonic devices (Barnes, Dereux et al. 2003). SPPs with large coherent length are useful in many areas, including optical processing, quantum information (Kamli, Moiseev et al. 2008) and novel light-matter interactions (Vasa, Pomraenke et al. 2008). The enhancement of local fields by SPPs is particularly crucial to absorption enhancement (Andrew, Kitson et al. 1997), nonlinear optical amplification (Coutaz, Neviere et al. 1985; Tsang 1996) and weak signal probing (Kneipp, Wang et al. 1997; Nie & Emory 1997). Although SPP only exists in the visible and near-infrared regimes where free conduction-band electrons on a metal surface are driven by external fields, its analogue can be found in other frequencies where surface charge-density wave does not exists. With induced surface current oscillations on an array of metallic building blocks (Pendry, Holden et al. 1996; Pendry, Holden et al. 1999; Sievenpiper, Zhang et al. 1999; Yen, Padilla et al. 2004; Hibbins, Evans et al. 2005; Liu, Genov et al. 2006; Lockyear, Hibbins et al. 2009), a metamaterial surface can manipulate electromagnetic waves in a similar way as SPPs. Such spoof SPPs or surface resonance states on a meta-surface can be tuned by geometric parameters.

We will summarize our recent studies on planar metamaterials covering the modal expansion theory (Sheng, Stepleman et al. 1982; Lalanne, Hugonin et al. 2000; Wei, Fu et al. 2010; Wei, Li et al. 2010; Wei, Cao et al. 2010; Wei, Cao et al. 2011), the broadband enhanced

transmission (Wei, Cao et al. 2011), negative refraction and subwavelength imaging (Wei, Cao et al. 2010), and the coherent control of spontaneous emission radiations in a wide frequency range (Wei, Li et al. 2010).

2. Broadband response of planar metamaterial

We introduce briefly the modal expansion method developed for multi-layered planar metamaterials in 2.1, and discuss the broadband enhanced transmission through holey metallic multi-layers (Wei, Cao et al. 2011), broadband negative refraction and subwavelength imaging in fishnet stacked metamaterial (Wei, Cao et al. 2010)in 2.2. In Section 2.3, we examine the properties of surface resonance states at a dielectric-metamaterial interface that exhibit magnetic response to the incident waves and strong local field enhancement (Wei, Li et al. 2010). We will show that a thin metamaterial slab, with a thickness much smaller than the operational wavelength, supports delocalized magnetic surface resonance states with a long coherent length in a wide range of frequencies. Operating in a broad frequency range, these spatially coherent SPPs are surface resonance states with quasi-TEM modes guided in the dielectric layer that are weakly coupled to free space, and the coupling strength can be controlled by tuning structural parameters while the frequency can be controlled by varying structural and material parameters. The high fidelity of these surface resonance states results in directional absorptivity or emissivity, which is angle-dependent with respect to frequency. These surface resonance states can give highly directional absorptivity and emissivity, and may thus help to realize interesting effects such as spatially coherent thermal emission, low-threshold plasmon lasing and sensitive photo-electric detection (Cao, Wei et al. 2011).

2.1 A method of modal expansion for planar metamaterials

The MEM is advantageous for analysis of electromagnetic transportation in planar metamaterial with layered geometry. The essence of MEM is to expand local EM fields in each layer as a series of in-plane envelope functions of eigenmodes. Let's demonstrate the formalism of MEM by solving the transmission spectra through one-dimensional metallic lamellar gratings with a thickness of h, as shown in Fig. 1. For simplicity, metals are treated as perfectly electric conductors (PEC) and EM waves only exist in apertures with the metallic layer.

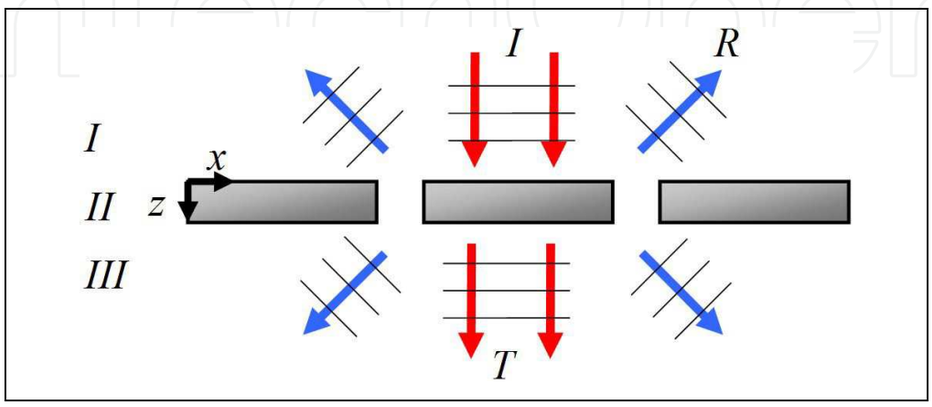

Fig. 1. Schematic of a one-dimensional metallic lamella grating.

For a transverse magnetic (TM) polarized incidence from the free semi-space at $z<0$ (region I), the total magnetic fields in region I and region II ($z>h$), which are along x direction, can be expressed in terms of incidence, reflection and transmission coefficients D0, Rm and Tm, as

$$H_1 = \left[D_0 \exp(jk_{z,0}z) + \sum_{m=-\infty}^{+\infty} R_m \exp(-jk_{z,m}z) \right] \exp\left(ik_0 \sin\theta x\right)$$

$$H_3 = \sum_{m=-\infty}^{+\infty} T_m \exp(jk_{z,m}z) \exp\left(ik_0 \sin\theta x\right) \tag{1}$$

Where $k_{z,j}^i$ denotes m^{th} order of Bloch wave vector in region i (i=1,2,3), θ is the incident angle. In region II of metallic lamellar gratings, the magnetic field can be written as the expansion coefficients a_l and b_l of forward and backward guided aperture modes, as

$$H_2 = \sum_{l=0}^{\infty} g_l(x) \left[a_l \exp\left(-jk_{z,l}z\right) + b_l \exp(jk_{z,l}z) \right] \tag{2}$$

where $g_l(x)$ is in-plane evelope function of waveguide mode of metallic layer. Under the as sumption of PEC for metalis, it can be expressed analytically as

$$g_l(x) = \begin{cases} \cos\left(\dfrac{\pi l}{w_x}x\right), & when \quad -\dfrac{w_x}{2} < x < \dfrac{w_x}{2} \\ 0, & else \end{cases} \tag{3}$$

By applying boundary continuum conditions at $z=0$ and $z=-h$ of the metal-air interfaces, we can obtain

$$\begin{cases} \underline{\Omega}(D_0 + \vec{R}) = \vec{a} + \vec{b} \\ D_0 - \vec{R} = \underline{\chi}(\vec{a} - \vec{b}) \\ u\vec{a} + u^{-1}\vec{b} = \underline{\Omega}(\vec{T} + \vec{R}) \\ \underline{\chi}(u\vec{a} - u^{-1}\vec{b}) = \vec{T} - \vec{R} \end{cases} \tag{4}$$

where $\Omega_{m,l}$, $\chi_{l,m}$ are the overlap integral of the projection between waveguide modes of metallic layers and Bloch modesin dlectric layers or free space, and can be expressed as

$$\begin{cases} \Omega_{m,l} = \dfrac{\int_{-p/2}^{p/2} e^{iG_m x} g_l^*(x)dx}{\int_{-p/2}^{p/2} g_l(x)g_l^*(x)dx} \\ \chi_{l,m} = \dfrac{\int_{-p/2}^{p/2} g_l(x)e^{-iG_m x}dx}{\int_{-p/2}^{p/2} e^{-iG_m x}e^{iG_m x}dx} \end{cases} \tag{5}$$

The coefficients a_l and b_l of forward and backwardwaveguide modecan be derived by Solving EQ.4, as

$$\begin{cases} \vec{a} = \dfrac{M_b^{-1}}{M_b^{-1} \bullet M_a - M_d^{-1} \bullet M_c} 2\underline{\Omega}\vec{D} \\ \vec{b} = \dfrac{M_a^{-1}}{M_a^{-1} \bullet M_b - M_c^{-1} \bullet M_d} 2\underline{\Omega}\vec{D} \end{cases} \tag{6}$$

where

$$\begin{cases} M_a = I + \underline{\Omega}\underline{\chi} \\ M_b = I - \underline{\Omega}\underline{\chi} \\ M_c = [I - \underline{\Omega}\underline{\chi}]u \\ M_d = [I + \underline{\Omega}\underline{\chi}]u \end{cases} \tag{7}$$

One advantage of MEM is that the problem can be solved without solving the inverse matrix of $\Omega_{m,l}$, $\chi_{l,m}$ so that the order of plane waves and that of waveguide modes are not necessarily be the same. At wavelength much larger than the array period, an $l \neq 0$ high order mode is evanescent and contribute little to transmission and reflection as the z component of wavevector is a large imaginary number.And the calculation is quickly convergent by adopting only a few waveguide modes.We can also see from Fig.2 that the calculated transmission spectra converge qucikly with only 7 plane waves considered as well.

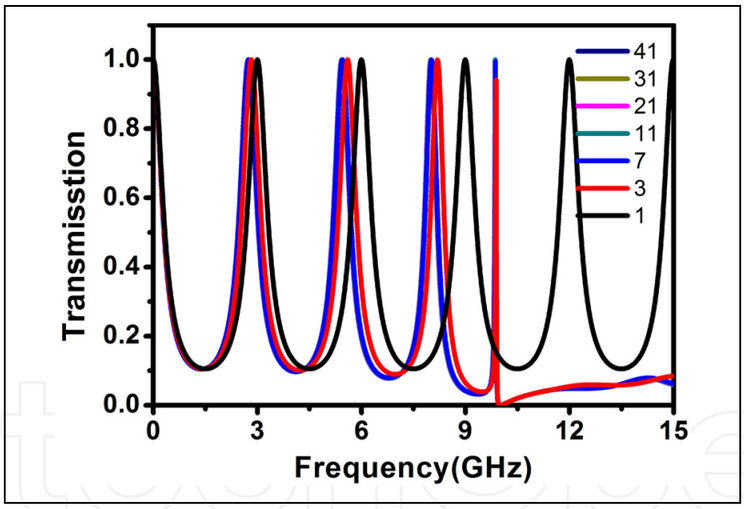

Fig. 2. Calculated 0th-order transmittance through the grating with different numbers of plane wave considered.

It is noticeable that the inter-layer coupling of EM waves can be analytically dealt with projection integral between the in-plane eigenmode functions of two adjacent layers. Under the treatment of MEM, a three-dimensional EM calculation will be simplified to a problem in two dimension. Thus the semi-analytical method is much faster than the conventional numerical simulations such as finite-difference-in-time-domain (FDTD) method, finite-element method etc. For metallic gratings, holey mesh, coaxial and split-ring structures, the method is quickly convergent by adopting only one or a few guided modes of metallic layers. The results shown in Fig.2 can be accomplished on an ordinary PC within a second,

which is several orders faster than any other numerical methods. The method can, in principle, be generalized to a layered metallo-dielectric structure perforated with arbitrary shaped apertures as the in-plane functions of eigenmodes within each layer can always be solved by a standard algorithm for eigenvectors of a two-dimensional system.

2.2 Broadband transparency from stacked metallic multi-layers perforated with coaxial annular apertures

Extraordinary optical transmission (EOT) through metallic film perforated with subwavelength hole arrays has attracted considerable attentions since the pioneering study by T.W. Ebbesen and his coworkers (Ebbesen, Lezec et al. 1998; Ghaemi, Thio et al. 1998). Substantial efforts have been devoted to exploring the physical origin of EOT, both theoretically and experimentally, due to the appealing prospect in related applications (Martin-Moreno, Garcia-Vidal et al. 2001; de Abajo & Saenz 2005; Gay, Alloschery et al. 2006; Liu & Lalanne 2008; Xiao, Jinbo et al. 2010; Bahk, Park et al. 2011). Previous studies extensively investigated the EOT effects arising from the resonant tunneling of surface plasmon polaritons (SPPs) (Raether 1988; Barnes, Dereux et al. 2003) through the perforated metallic film. The frequency of such an EOT transmission peak is not only scaled to the period of hole arrays, but also very sensitive to the incident angle as the resonant tunneling occurs via the in-plane Bragg-scattering channels. Very recently, similar phenomena of the EOT through cascaded metallic multi-layers, which are perforated with one-dimensional gratings or two-dimensional hole arrays, have also been brought into attention (Miyamaru & Hangyo 2005; Ye & Zhang 2005; Chan, Marcet et al. 2006; Tang, Peng et al. 2007; Ortuno, Garcia-Meca et al. 2009; Marcet, Hang et al. 2010; Zhou, Huang et al. 2010). The resonant coupling among the SPP modes on different layers can be tuned by the spacing distance and lateral displacement of hole arrays at different layers, leading to tunable transmission peaks and zeros in spectra. It is worth noting that, when the slit size is very large or some kinds of specific apertures are adopted, the waveguide resonant modes of a slit or aperture can also give rise to the phenomena of EOT by allowing electromagnetic waves to propagate through the metallic slab. The cut-off wavelength of guided resonance modes (Baida, Van Labeke et al. 2004; Fan, Zhang et al. 2005; Fan, Zhang et al. 2005; van der Molen, Klein Koerkamp et al. 2005; Wen, Zhou et al. 2005; Wei, Fu et al. 2010) is primarily determined by the geometry of slits or apertures, and thus can be much longer than the array period. Under this circumstance, the EOT can also occur at a rather low frequency which is not scaled to the array period,and is robust against the structure disorder (Ruan & Qiu 2006). To the best of our knowledge, the EOT of metallic multi-layers arising from guided resonance modes has not yet been investigated before.

Here, we investigate the enhanced transmission of metallic multi-layers perforated with periodic arrays of coaxial annular apertures (CAAs). Modal expansion method (MEM) is developed to semi-analytically deal with the electromagnetic properties of the multilayered system. We show that the hybridization of guided resonance modes of CAAs in adjacent layers dramatically extends an enhanced transmission peak into a broad passband that is nearly reflectionless. The passband gets more and more broadened with sharper edges when the system contains more metallic layers. In contrast, these results can not be observed when the wave propagation is dictated by evanescent coupling of SPP modes (Miyamaru & Hangyo 2005; Ye & Zhang 2005; Chan, Marcet et al. 2006; Tang, Peng et al. 2007; Ortuno, Garcia-Meca

et al. 2009; Marcet, Hang et al. 2010; Zhou, Huang et al. 2010). Measured transmission spectra are in good agreement with calculations for the model systems with different metallic layers. The broadening and varied fine structures of the EOT passband with the increase of metallic layers,can be understood intuitively by a physical picture of mode splitting of coupled atoms. The passband of the enhanced transmission for a system with only two or three metallic layers, covering a wide frequency range with sharp band-edges, can be estimated by calculated dispersion diagram under the assumption of infinite metallic layers.

A model system with n metallic layers perforated with square arrays of CAAs is of our interest. Figure 3 presents the front-view photo and schematic configuration of a sample with three thin metallic layers ($n=3$) and two sandwiched dielectric space layers. The aperture arrays deposited on different layers are aligned with no displacement in xy plane. The geometric parameters are the lattice constant $p=10\text{mm}$ of square arrays, the outer radius $R=4.8\text{mm}$ and inner radius $r=3.8\text{mm}$ of CAAs, and the thickness $t=0.035\text{mm}$ of metallic layer respectively. Each dielectric layer has a thickness of $h=1.575\text{mm}$ and a permittivity of $\varepsilon_r=2.65$.

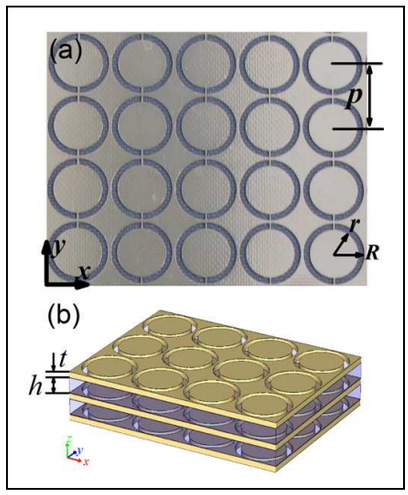

Fig. 3. (a) Top-view photo and (b) 3D schematic of our sample with three metallic layers (n = 3). The metallic layers are perforated with coaxial annular apertures (CAAs).

Under assumption of perfect electric conductor (PEC) for metals, the electromagnetic wave fields within a metallic layer only exist in apertures. In cylindrical coordinate system, the radial and angular field components E_ρ and E_ϕ inside an aperture of the metallic layer can be analytically expanded by the superposition of guided resonance modes of the aperture, as

$$E_\rho(\rho,\phi,z)=\sum_{l=1}^{\infty}(a_l e^{-i\beta_l z}+b_l e^{i\beta_l z})g_l(\rho,\phi)$$

$$E_\phi(\rho,\phi,z)=\sum_{l=1}^{\infty}(a_l e^{-i\beta_l z}+b_l e^{i\beta_l z})f_l(\rho,\phi)\,, \tag{8}$$

where a_l and b_l are the coefficients of forward and backward guided waves inside the CAAs,

$$g_l(\rho,\phi) = \frac{j\omega\mu l}{\rho}\left[N'_l(T_l r)J_l(T_l\rho) - J'_p(T_l r)N_l(T_l\rho)\right]\sin(l\phi)$$

and $$f_l(\rho,\phi) = j\omega\mu T\left[N'_l(T_l r)J'_l(T_l\rho) - J'_p(T_l r)N'_l(T_l\rho)\right]\cos(l\phi)$$

are the l^{th} order modal functions of radial and angular components in aperture with $J_l(x)$ and $N_l(x)$ being the l^{th} order Bessel and Neumann functions, T_l refers to the root of the equation $J'_l(TR)N'_l(Tr) - J'_l(Tr)N'_l(TR) = 0$. By adopting EQ. (8) as expressions of EM fields in metallic layers and plane-waves as those in dielectric layers, we perform MEM to resolve the electromagnetic problems in the multilayered system. The method is quickly convergent by considering only 2 or 3 lowest guided resonance modes of CAAs. A higher order resonance mode contributes little to the interlayer coupling as its wave vector β_l is a large imaginary number. Three guided modes ($l = 1,2,3$) in CAAs and 11×11 orders of plane-wave basis in dielectric layers are adopted in our calculations. The results are very accurate (solid lines in Fig.4) and in good agreement with the measurements (circular dots in Fig.4).

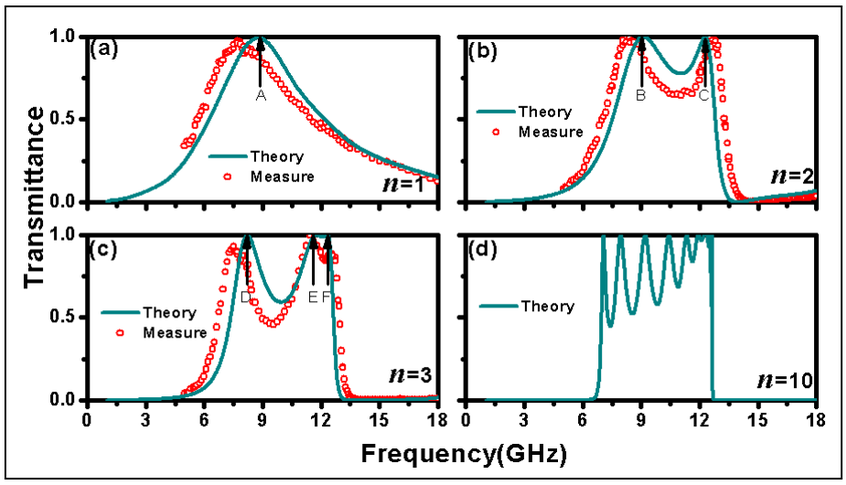

Fig. 4. Transmission spectra through the models with (a) n=1, (b) n=2, (c) n=3, (d) n=10 metallic layers. Solid lines for calculated results by Modal expansion method (MEM), circular dots for measured results in microwave regime.

We see from Fig. 4 (a) that there exists a transmission peak for the n=1 sample at $f_A = 8.7\text{GHz}$ due to the excitation of guided TE_{11} resonance mode in CAAs. We also see from Figs. 4 (b) and 4 (c) that there are two transmission peaks at $f_B = 9.1\text{GHz}$, and $f_C = 12.3\text{GHz}$ for the $n = 2$ sample, three peaks at $f_D = 8.2\text{GHz}$, $f_E = 11.64\text{GHz}$ and $f_F = 12.35\text{GHz}$ for the $n = 3$ sample. Figure 4 (d) presents the calculated transmission spectra of an n=10 model system. It means that, with the increase of metallic layers, more transmission peaks emerge, giving rise to a broad transparent band.

More calculations show that, for the $n = 2$ sample, at an on-resonance frequency $f_B = 9.1\text{GHz}$ or $f_C = 12.3\text{GHz}$ where transmissivity is nearly unity, the spatial distribution of electric fields [see Figs. 5 (a) and 5 (b)] are symmetric or anti-symmetric about the xy plane. And the transmitted waves possess a phase difference of 0 (in phase) or π (out phase) with respect to the incident waves. Therefore the peaks at f_B and f_C, derived

from the peak at f_A of the $n=1$ model, come from the excitation and hybridization of the TE_{11} guided resonance modes in apertures at different metallic layers as a results of mode splitting of coupled apertures (or meta-atoms). Further more, the anti-symmetric mode at $f_C=12.3\text{GHz}$ of the $n=2$ model splits into two modes of the $n=3$ model: spatial field distribution of the one at $f_E=11.64\text{GHz}$ reveals that the incident and outgoing waves are out phase to each other [Fig. 5 (d)] and it is on the opposite for the other at $f_F=12.35\text{GHz}$ [Fig.5 (e)], while the resonant mode at the lowest frequency $f_D=8.2\text{GHz}$ retains a symmetric feature in field distribution [Fig. 5 (c)] and inherits the in-phase signature from the symmetric mode at f_B of the $n=2$ model.

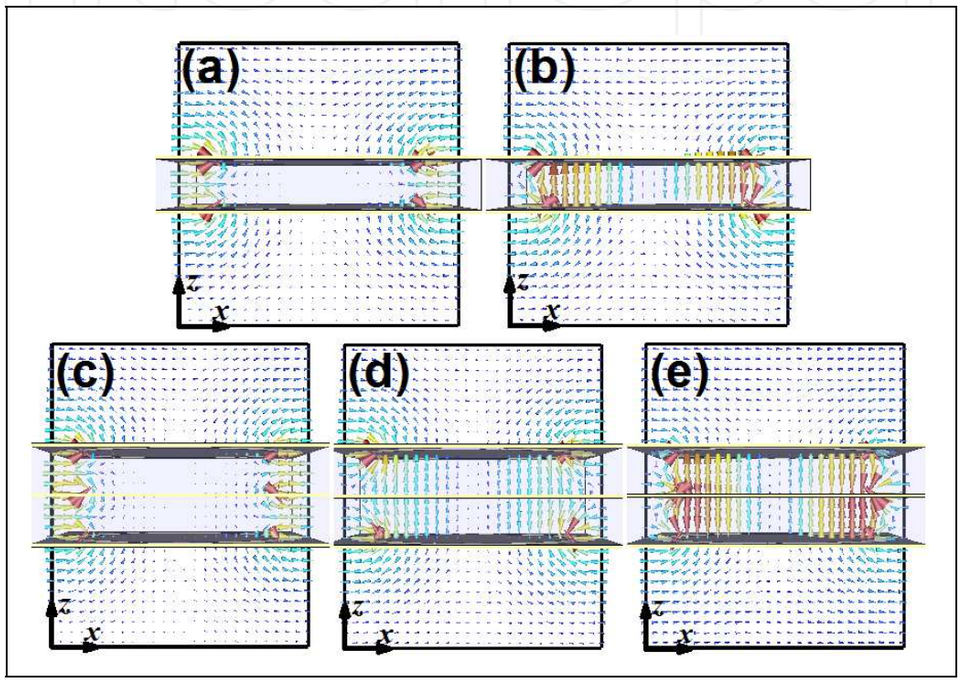

Fig. 5. Spatial distribution of electric fields in the xz plane at on-resonance frequencies of (a) f_B = 9.1GHz, (b) f_C = 12.3GHz for the n = 2 model , and (c) f_D = 8:2GHz, (d)f_E = 11.64GHz, (e) f_F = 12.35GHz for the n = 3 model.

Figure 6 (a) presents the dispersion relation of bulk material periodically constructed with layered CAAs. The band structure is calculated with MEM algorithm assuming periodic boundary conditions along the z axis. The process of mode splitting from $n=1$ to $n=3$, as shown in Fig. 6 (b), depicts the evolution of the enhanced transmission feature from a single transmission peak to a broad passband. It is interesting that the passband between $f_b=6.77\text{GHz}$ and $f_t=12.7\text{GHz}$ shown in Fig. 6 (b), predicting the passband of the n=10 model quite well, is also a good measure of the bandwidth of the n=3 sample. The total bandwidth is about 60% of the central frequency. In contrast, the EOT observed in multilayered systems of previous studies demonstrates a peak lineshape in spectra as it arises from the resonant tunneling of SPP modes among metallic films instead of guided resonance modes. And the broad passband we observed is not sensitive to the incident angle (not shown), while it is on the contrary when the SPP modes dominate.

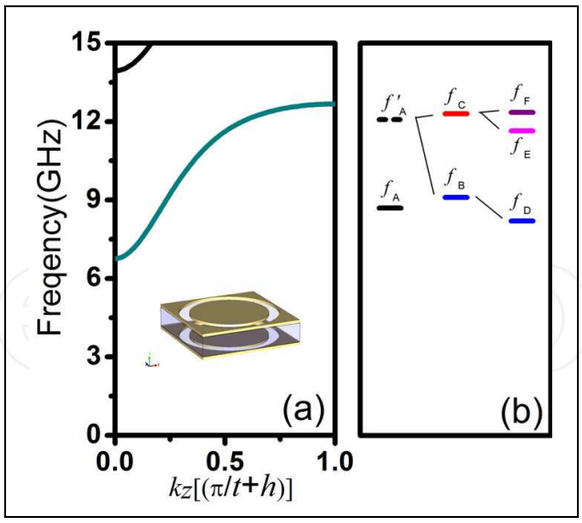

Fig. 6. Transmission spectra through the models with (a) n=1, (b) n=2, (c) n=3, (d) n=10 metallic layers. Solid lines for calculated results by Modal expansion method (MEM), circular dots for measured results in microwave regime.

This work reports for the first time that enhanced transmission peak can be broadened through stacked metallic multi-layers perforated with CAAs. Taking advantage of the excitation of guided resonance modes of CAAs and interlayer coupling, the enhanced transmission of such a system with only three metallic layers can span a wide frequency range covering about 60% of the central frequency. The broadband utility shall have enormous potential applications in optoelectronics, telecommunication and image processing.

2.3 Broadband negative refraction from stacked fishnet metamaterial

Since J.B. Pendry proposed perfect lens (Pendry 2000) using left-handed materials (Veselago 1968), sustained attentions have been drawn to the negative-index metamaterial (NIM) with simultaneously negative permittivity and permeability. The NIM, comprising of subwavelength metallic resonant units, has been designed and realized in both the microwave (Shelby, Smith et al. 2001) and optical regime (Liu, Guo et al. 2008). Negative refraction and subwavelength imaging with NIMs have great application potentials in photonic devices (Grbic & Eleftheriades 2004; Belov, Hao et al. 2006; Wiltshire, Pendry et al. 2006; Freire, Marques et al. 2008; Silveirinha, Fernandes et al. 2008; Silveirinha, Medeiros et al. 2010). Among various types of NIMs, one most promising candidate is the so-called fishnet NIM which comprises of alternating metal/dielectric layers perforated with two-dimensional array of holes (Beruete, Campillo et al. 2007; Beruete, Sorolla et al. 2007; Beruete, Navarro-Cia et al. 2008; Navarro-Cia, Beruete et al. 2008; Navarro-Cia, Beruete et al. 2009). The simple structure also provides a feasible solution for optical NIM (Dolling, Enkrich et al. 2006; Zhang, Fan et al. 2006; Dolling, Wegener et al. 2007; Valentine, Zhang et al. 2008; Ku & Brueck 2009; Ku, Zhang et al. 2009).

In most of the previous studies on fishnet NIMs (Dolling, Enkrich et al. 2006; Zhang, Fan et al. 2006; Beruete, Campillo et al. 2007; Beruete, Sorolla et al. 2007; Dolling, Wegener et al.

2007; Beruete, Navarro-Cia et al. 2008; Navarro-Cia, Beruete et al. 2008; Valentine, Zhang et al. 2008; Ku & Brueck 2009; Ku, Zhang et al. 2009; Navarro-Cia, Beruete et al. 2009), the light waves are incident on the top interface of the metal/dielectric multi-layers. Thus the light waves can not penetrate into the structure below the cut-off frequency of air holes, and the negative index was retrieved only within in a narrow frequency range above the cut-off. In this section, a different incidence configuration is employed by impinging the light waves on the sidewall interface of fishnet NIM that is perpendicular to the metal/dielectric multi-layers. As the uniformly spaced holey metallic layers of fishnet NIM constitute a multiple of slab waveguide channels filled with dielectric spacer layers, the incidence configuration of this kind enables us to fully exploit the optical properties of the fishnet NIM in the long wavelength limit. We show that the evanescent coupling between the slab waveguides gives rise to all-angle negative refraction and sub-wavelength imaging in a wide frequency range starting from zero.

Figure 7 schematically illustrates the structure of our stacked fishnet metamaterial and the incidence configuration. The metal/dielectric layers are lying in $\hat{x}\hat{y}$ plane. The square arrays of air holes perforated on metallic layers are aligned along z axis without lateral displacement in $\hat{x}\hat{y}$ plane. The period of the hole array, the thickness of metallic layer and dielectric layer are p=6.0mm, t=0.035mm and h=1.575mm respectively. The line width of metallic strips along x direction w=0.2mm is the same as that along y direction, and the size of square holes is a=p-g=5.8mm. The dielectric constant of the dielectric layer is ε_r =2.55. The EM incidence waves are propagating in the $\hat{x}\hat{z}$ plane with an incident angle of θ.

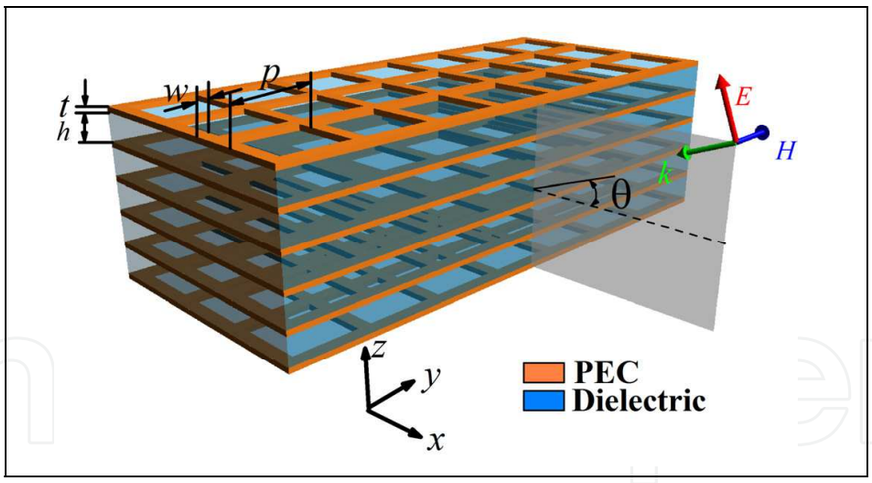

Fig. 7. The schematic of stacked fishnet metamaterial. The red and blue arrows refer to the directions of electric field $\vec{E}$ and magnetic field $\vec{H}$. The plane in gray color denotes the incident plane.

Figure 8 presents the calculated dispersion diagram along the Γ (0,0,0)→X (0.5,0,0), Γ (0,0,0)→M (0.5,0,0.5) and M (0.5,0,0.5)→X (0.5,0,0) directions. The blue dashed line refers to the light line in dielectric. We notice that, the lowest branch along the ΓX direction ($k_z = 0$) precisely reproduces the light line in dielectric. This is understandable with the help of modal expansion method. Detailed calculations show that these $k_z = 0$ states only

contain the 0th order Bloch component which is the transverse electromagnetic (TEM) mode that is always orthogonal to the local modes of air hole. In this situation, the free photons in the dielectric are the only choice for the $k_z = 0$ states as no evanescent couplings happen via the breathing air holes. However the lowest branch ($k_z \neq 0$) along the ΓM and XM directions (red solid line in Fig.8) evidently deviates from the light line in dielectric. The $k_z \neq 0$ states on this branch originate from the evanescent coupling between the adjacent slab waveguides via the TE_{10} mode of holes (noting that the overlap integral between a high order of guided Bloch mode and local mode of air hole is not zero). Figure 9 (a) presents the charts of equi-frequency surface (EFS) analysis for the $k_y = 0$ states to further reveal the characteristics of this band. All curves in Fig. 9 (a) are in a hyperbolic-like lineshape, which indicates that all-angle negative refraction occurs in the $\hat{x}\hat{z}$ plane at low frequency regime starting from zero. At lower frequency the curves in Fig. 9 (a) become much more flat, which means that the waves are also strongly collimated inside the structure along the direction parallel to the metal/dielectric layers. A numerical proof of negative refraction is shown in Fig. 9 (b). In our FDTD simulations, a monochromatic one-way Gaussian beam in the $\hat{x}\hat{z}$ plane with a frequency at 11GHz is incident from upside at an incident angle of 30o. The fishnet model is stacked with 500 metal/dielectric layers along z direction. Given the periodicity of hole arrays and the incidence configuration, 60 periods along x direction and one period along y direction are adopted for the metal/dielectric layers in space domain. The negative refraction is clearly shown in Fig. 9 (b) with the magnetic field distribution in xz plane. The black arrows denote the directions of energy flow in the free space and fishnet structure. A refraction angle of -16.2o, retrieved from the refracted direction of the energy flow or the negative Goos-Hanchen shift alternatively, is in good agreement with the estimate in EFS analysis. We also see from Fig. 9 (b) that almost no reflection occurs as the incidence can easily propagates inside the structure by coupling with the guided Bloch modes in the slab waveguide channels.

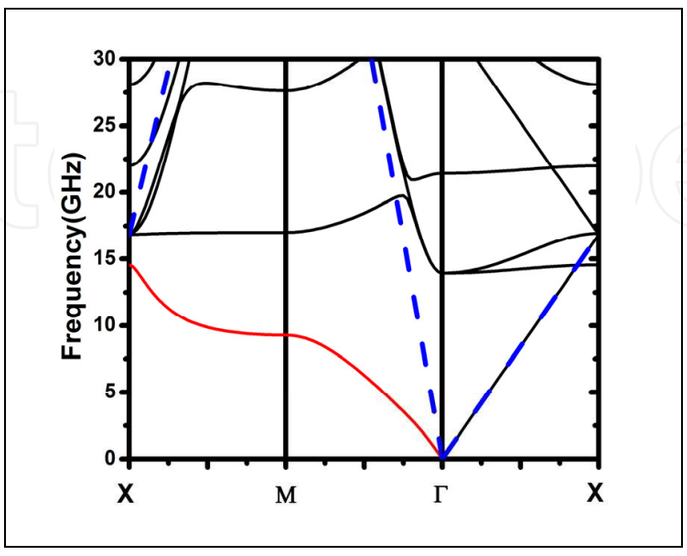

Fig. 8. The dispersion diagram of the stacked fishnet metamaterial.

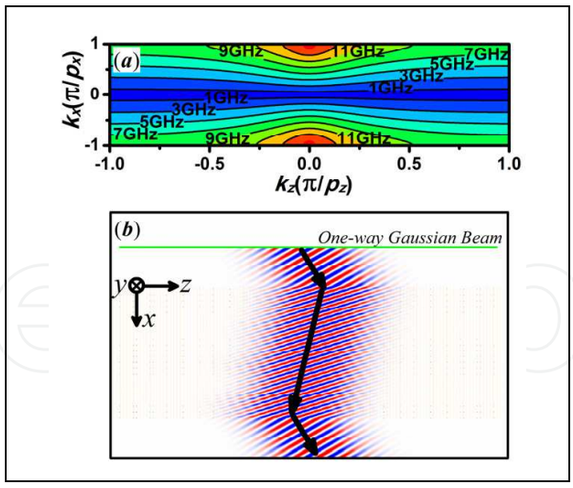

Fig. 9. (a) The charts of EFS analysis for ky=0 states respect to k_z and k_x . (b) The FDTD simulations on the magnetic field distribution in the problem domain. The one-way Gaussian beam is about 70mm away from the top interface of our fishnet model.

The optical properties of such a system can be described with the coupled wave equation (Haus & Molter-Orr 1983; Eisenberg, Silberberg et al. 2000; Pertsch, Zentgraf et al. 2002) by considering the coupling between the n^{th} waveguide channel and its nearest neighbors, the $(n\text{-}1)^{th}$, $(n+1)^{th}$ waveguide channels, as:

$$i\frac{da_n(x)}{dx} + \beta a_n(x) + C[a_{n+1}(x) + a_{n-1}(x)] = 0 \tag{9}$$

Where $a_n(x)$ denotes the wave fields in the n^{th} slab waveguide, C is the coupling coefficient, and β is the propagation constant of free photons in dielectric. Under the periodic boundary condition along z direction, the dispersion of the system takes the form as

$$k_x = \beta + 2C\cos(k_z p) \tag{10}$$

where k_x and k_z are the vector components along the x and z directions. At $k_z = 0$, the coupling coefficient $C = 0$ is zero (as aforementioned no evanescent coupling occurs) and we have $k_x = \beta$ which is rightly the light line in the dielectric. While C is always negative when $k_z \neq 0$ in the limit of long wavelength [which can be deduced from the charts in Fig. 8 (a)], giving rise to all-angle negative refraction. We note that the silver/dielectric multi-layered structure also supports all-angle negative refraction in a certain optical frequency regime under the same incidence configuration of our study (Fan, Wang et al. 2006). The long range SPPs play an important role for the negative refraction. We also note that, at long wavelength limit, a holey metallic surface can be homogenized into a single-negative medium with electric response in the form of Drude model (Pendry, Martin-Moreno et al. 2004). The plasmon frequency is rightly the cut-off frequency of air holes. Thus it is reasonable for us to consider the stacked fishnet metamaterial as an artificial plasmonic waveguide array. The negative coefficient C implies that for the eigenstates on the lowest branch, the spatial field distributions are anti-symmetric with respect to the plane of air

holes. If our findings are applicable in optical regime, the most field energy shall propagate outside the lossy metal film with anti-symmetric field distribution, and low loss is expected. The picture may be helpful as well to explain the low loss measured in a recent experiment about fishnet optical NIMs (Zhang, Fan et al. 2006; Valentine, Zhang et al. 2008).

One important application of all-angle negative refraction is flat lens. The imaging performance of our stacked fishnet metamaterial is examined by the brute-force FDTD numerical simulations. As shown in Fig.10, a monochromatic point source with a frequency at 11GHz is located 15mm away from the surface at the left side of the fishnet structure. The snap shot shown in Fig. 10 (a) clearly indicates a high-quality image achieved at another side of the structure about 15mm away from the interface. The image resolution can be checked by the normalized magnetic field profile at image plane. As illustrated in Fig. 10 (b), along z axis, the full width at half maximum (FWHM) of the field profile is 10mm about one-third of the wavelength. The FWHM at a lower frequency still remains at about 10mm, leading to a better resolution in subwavelength scale along the z direction. But a longer structure is required due to strong collimation effect at lower frequency.

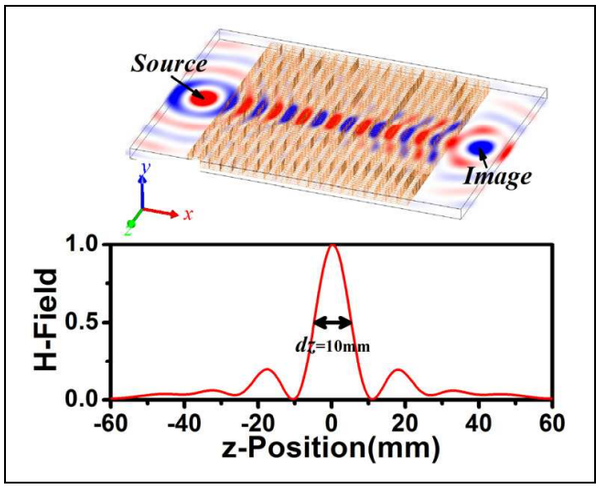

Fig. 10. (a) The snap shot of magnetic field distribution in the incident plane. The model, stacked with 80 metal/dielectric multi-layers along z axis, has 20 periods along x direction and one period along y direction. (b) Normalized magnetic field profile at the source plane (black solid line) and the image plane (red solid line) as a function of the z aixs

In conclusion, the fishnet metamaterials can operate as plasmonic waveguide arrays. The broadband negative refraction, subwavelength imaging in the long wavelength limit have great potentials for photonic devices in microwave, THz and even in the optical regimes.

2.4 Spatially coherent surface resonant states derived from magnetic meta-surface

Surface plasmon polaritons (SPPs) can modulate light waves at the metal-dielectric interface with wavelength much smaller than that in free space (Raether 1988),which enables the control of light in a subwavelength scale for nanophotonic devices (Barnes, Dereux et al. 2003). SPPs with large coherent length are useful in many areas, including optical processing, quantum information (Kamli, Moiseev et al. 2008) and novel light-matter

interactions (Vasa, Pomraenke et al. 2008). The enhancement of local fields by SPPs is particularly important as it opens a new route to absorption enhancement (Andrew, Kitson et al. 1997), nonlinear optical amplification (Coutaz, Neviere et al. 1985; Tsang 1996) as well as weak signal probing (Kneipp, Wang et al. 1997; Nie & Emory 1997). As the properties of SPP are pretty much determined by the natural (plasmon) resonance frequency, there is not much room for us to adjust the SPP response for practical applications. With induced surface current oscillations on an array of metallic building blocks (Pendry, Holden et al. 1996; Pendry, Holden et al. 1999; Sievenpiper, Zhang et al. 1999; Yen, Padilla et al. 2004; Hibbins, Evans et al. 2005; Liu, Genov et al. 2006; Lockyear, Hibbins et al. 2009), metamaterial surfaces can manipulate electromagnetic waves in a similar way as SPPs. Such SPPs or surface resonance states on structured metallic surfaces are tunable by geometric parameters.

Here, we examine the properties of surface resonance states at a dielectric-metamaterial interface that exhibit magnetic response to the incident waves and strong local field enhancement. We will see that these surface resonance states can give highly directional absorptivity and emissivity, and may thus help to realize interesting effects such as spatially coherent thermal emission. As the structure is very simple, it can be fabricated down to the IR and optical regime (Grigorenko, Geim et al. 2005; Shalaev 2007; Boltasseva & Shalaev 2008).

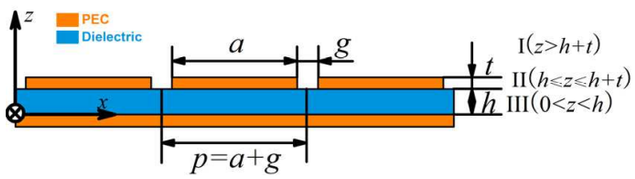

Fig. 11. Schematic picture of the magnetic metamaterial slab

We will show that a thin metamaterial slab, with a thickness much smaller than the operational wavelength, supports delocalized magnetic surface resonance states with a long coherent length in a wide range of frequencies. Operating in a broad frequency range, these spatially coherent SPPs are surface resonance states with quasi-TEM modes guided in the dielectric layer that are weakly coupled to free space, and the coupling strength can be controlled by tuning structural parameters while the frequency can be controlled by varying structural and material parameters. The high fidelity of these surface resonance states results in directional absorptivity or emissivity, which is angle-dependent with respect to frequency. Finite-difference-in-time-domain (FDTD) simulations verify that the highly directional emissivity from the slab persists in the presence of structural disorder in the grating layer.

Such metal-dielectric-metal (MDM) structures were recognized as artificial magnetic surfaces with high impedance by the end of last century [12]. The incident waves induce surface current solenoids on the unit cells of the ultra-thin high-impedance surface, giving rise to magnetic susceptibilities. The magnetic response can be described with an effective permeability in Lorentz type (Sievenpiper, Zhang et al. 1999; Zhou, Wen et al. 2003). After the concept of metamaterial being proposed (Engheta & Ziolkowski 2006), P. Alastair and

his co-workers numerically and experimentally proved that the ultra-thin MDM structures can resonantly absorb or transmit radiations at low frequency limit (Hibbins, Sambles et al. 2004). They addressed that the central frequencies of absorption peaks are independent from the incident angle with an interpretation of Farby-Perrot resonant mode (EQ. 1 in Ref. 22). The same group further explored the angle-independent absorption, as the main scenario of the incremental work, by measuring the flat bands of surface wave dispersion in the visible (Hibbins, Murray et al. 2006) as well as the microwave region (Brown, Hibbins et al. 2008). In contrast, we find that the structures with proper design also supports very narrow absorption peaks which are sensitiveto the incident angle and obviously do not satisfy to the Fabry-Perot resonance condition suggested in the previous studies.

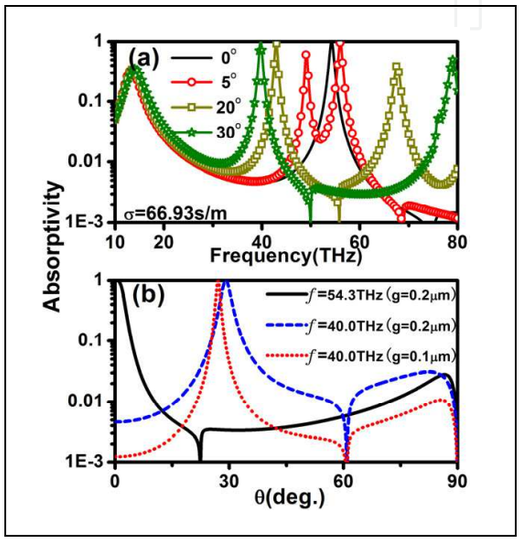

Fig. 12. Absorption spectra under TM-polarized incidence (a) as a function of frequency at incident angles of $\theta = 0^o, 5^o, 20^o, 30^o$ (g=0.2μm) and (b) as a function of incident angle at 54.3THz (solid line, g=0.2μm), 40THz (dashed line, g=0.2μm) and 40THz (doted line, g=0.1μm)

It is worth noting that an angle-independent peak is quite different from an angle-dependent one in physics origin. The former, investigated in Refs. 22-24, comes from the localized surface resonance states, while the latter, found by us, comes from the collective surface resonance states. Mode analysis presents An an intuitive picture for the formation of these collective surface states. When high order quasi-TEM modes are dominant components of the guided waves inside the dielectric layer they will assign phase correlation to the outgoing waves emitted from the air slits of grating, thus are very crucial to the formation of collective response. Weak enough both the leakage from dielectric layer to air slits and the material absorption, the spatial coherence of surface resonant states will survive. As the interaction between the structure and the incident waves will excite quasi-TEM modes inside the dielectric layer, the magnetic induction must be parallel to the MDM surfaces if it exists. Thus a surface resonant state on a MDM structure is usually magnetic in nature. Our findings about spatially coherent surface resonance states are original compared to the common knowledge, and have great potentials in coherent control of SPPs as well as thermal emission radiations.

Our model system is schematically illustrated in Fig. 11. Lying on the $\hat{x}\hat{y}$ plane, the slab comprises an upper layer of a metallic lamellar grating with thickness *t*, a dielectric spacer layer as a slab waveguide with thickness *h* and a metallic ground plane. The metallic strips are separated by a small air gap *g*, giving rise to a period of *p*=*a*+*g* for the lamellar grating. The geometric parameters of our model are $t = 0.2\mu m$, $h = 0.8\mu m$, $a = 3.8\mu m$, $g = 0.2\mu m$ and $p = a + g = 4.0\mu m$. Each metallic strip together with the ground plane beneath it constitutes a planar resonant cavity as the building block that gives magnetic responses at cavity resonances (Sievenpiper, Zhang et al. 1999; Lockyear, Hibbins et al. 2009). As the metallic grating is along the $\hat{x}$ direction, the guided waves in the dielectric layer (at $0 < z < h$ in region III) shall always couple to the incident waves with a non-zero component $E_x \neq 0$ of electric field.

As a first step, we consider a transverse magnetic (TM) polarized incident plane wave in the free semi-space (at $z > h + t$ in region I). The electric field $\vec{E}$ lies in $\hat{x}\hat{z}$ plane, the magnetic field $\vec{H}$ is along y axis and the in-plane wave vector is $\vec{k}_{0_{\parallel}} = k_x \hat{e}_x$ ($k_y = 0$). The total magnetic fields in region I and in region III can be written in terms of the reflection coefficients r_m and the guided Bloch wave coefficients t_m , as

$$\begin{aligned} H_y^I(\vec{r},z) &= \delta_{m,0} e^{-ik^I_{z_m} z} e^{ik_x x} + \sum_m r_m e^{ik^I_{z_m} z} e^{i(k_x + 2m\pi/p)x} \\ H_y^{III}(\vec{r},z) &= \sum_m [t_m e^{ik^{III}_{z_m} z} + t_m e^{-ik^{III}_{z_m}(z-2h)}] e^{i(k_x + 2m\pi/p)x}, \end{aligned} \tag{11}$$

where the term $\delta_{m,0} e^{-ik^I_{z_m} z} e^{ik_x x}$ denotes the incident plane wave with $\delta_{m,0}$ being the Kronecker function and m being the Bloch order; $e^{i(k_x + 2m\pi/p)x}$ denotes wave component of the m^{th} Bloch eigenmode in the semi-free space (region I) and the dielectric layer (region III) with respect to $\vec{k}_m = \hat{x}(k_x + 2m\pi/p)$. $\vec{k}_m$ is the in-plane wave vector and $\vec{G}_m = \hat{x} \cdot 2\pi m/p$ is the m^{th} reciprocal lattice vector.

$$k^I_{z_m} = \sqrt{\varepsilon_0 \mu_0 \omega^2 - |\vec{k}_m|^2} \quad \text{and} \quad k^{III}_{z_m} = \sqrt{\varepsilon_{III} \mu_0 \omega^2 - |\vec{k}_m|^2}$$

are the z components of wave vector for the m^{th} order Bloch eigenmode in region I and region III respectively. ε_0 and ε_{III} are the permittivity of the vacuum and the dielectric , μ_0 is the vacuum permeability. In general, we also derived the method for a plane wave incidence with any specific wavevector and any specific polarization.

We shall mainly consider infrared frequencies, at which the metals can be well approximated as perfectly electric conductors (PEC). The EM fields at $h \le z \le h + t$ in region II are squeezed inside the air gaps, in which the magnetic fields can be expressed in terms of the expansion coefficients a_l and b_l of forward and backward guided waves, as:

$$H_y^{II}(\vec{r},z) = \sum_l [a_l e^{-iq_l(z-h-t)} + b_l e^{iq_l(z-h)}] g_l(x), \tag{12}$$

where $g_l(x) = \cos[l\pi/g(x + g/2)]$, $(l = 0,1,...,n,...)$ is the in-plane distribution of guided mode α_l running over all air gaps. $q_l = \sqrt{\varepsilon_0 \mu_0 \omega^2 - (l\pi/g)^2}$ is the z component of wave vector for the l^{th} guided mode α_l .

We can obtain the coefficients $t_m(f,\vec{k}_{0_{//}})$ and $r_m(f,\vec{k}_{0_{//}})$ of the m^{th} guided and reflected waves by applying the boundary continuity conditions for the tangential components of electromagnetic wave fields (over the slits) at the interfaces $z=h$ and $z=h+t$. Given that surface resonance modes are intrinsic response, we can also assign zero to the incident plane wave and apply the boundary continuity conditions for the tangential components of wave fields to derive the eigen-value equations. A surface resonance state can be determined by searching a zero value / minimum of eigen-equation determinant in the reciprocal space provided that it is non-radiative/radiative with infinite/finite life time below/above light line in free space.

We derived the absorption spectra of the slab

$$A(\vec{k}_0,\omega)=1-\sum_m \mathrm{Re}(\frac{k^I_{z_m}}{k^I_{z_0}})\,|\,r_m(\vec{k}_0,\omega)\,|^2$$

which includes the contributions from all Bloch orders of reflected waves. As a consequence, $A(\vec{k}_0,\omega)$ gives information about the surface resonance states as well as the emissivity properties as governed by Kirchhoff's law (Greffet & Nieto-Vesperinas 1998). We shall assume that the dielectric spacer layer is slightly dissipative by assigning a complex permittivity $\varepsilon_{III}=\varepsilon_r\varepsilon_0+i\sigma/\omega$ with $\varepsilon_r=2.2$ and $\sigma=66.93S/m$ [$\mathrm{Im}(\varepsilon_{III})\approx 10^{-2}\varepsilon_r\varepsilon_0$] in the calculated frequency regime. In Fig. 12 (a), we present the absorption spectra at various incident angles. The spectra exhibit a low and broad peak at *13.2*THz which is almost independent of the incident angle, while the other absorption peaks at higher frequencies are narrow and sensitive to the incident angle with a maximum absorption approaching 100%. The slab thus acts as an all-angle absorber at *13.2*THz, but exhibits sharp angle-selective absorption peaks at higher frequencies. Shown as solid and dashed lines in Fig. 12 (b), the sharp angular dependence of absorption coefficients (note that the vertical axis is in log-scale) at 40.0*THz* and 54.3THz implicitly implies the existence of spatially coherent surface resonance states. The angle-dependent absorption peaks become lower and disappear gradually with the increase of the material loss. This presents a way to realize nearly perfect absorption with weakly absorptive materials by coherent surface resonance states. The coherent length of a surface resonance state can be estimated by the ratio of the wavelength λ and the full width at half maximum (FWHM) $\Delta\theta$ of the absorption peak (Greffet, Carminati et al. 2002). For example, for the Γ_4 state at 54.3THz and $\vec{k}_{0_{\|}}=0$, the angular FWHM of the corresponding absorption peak $\Delta\theta=4.6^o$ (from $\theta=-2.3^o$ to $\theta=2.3^o$) gives rise to a coherent length $\lambda/\Delta\theta=68.5\mu m\approx 12.4\lambda$. The coherent length is about 220λ for the surface resonance state at 50.22THz and $\vec{k}_{0_{\|}}=0.01\pi/p$ with $\Delta\theta=0.26^o$ (not shown in figure). The angular FWHM is reduced if the gap size is smaller, as shown with the dashed and dotted lines in Fig.12 (b) for $g=0.2\mu m$ and $g=0.1\mu m$ at 40THz, which means that the coherent length of the surface resonant modes can be controlled by the gap-period ratio g/p. It is worth noting that, although k_y*=0* is assumed for the calculated results shown in Fig. 12, the angle-dependent absorption peaks are readily obtained for any specific incident angle.

To quantitatively characterize the formation of these spatially coherent surface resonance states, we employ the eigenmode expansion method to calculate the surface resonance

dispersion (in the limit of no material loss) as shown in Fig. 13 (b).The B_1 surface resonance states lie below the light line L_2 (magenta dashed line), and thus are non-radiative as evanescent modes. The surface resonances labeled as B_2 originate from the coupling of the fundamental magnetic resonance modes of the metal strip structure with the free space light line L_2. The surface resonances B_3 and B_4 are harmonic modes of the magnetic resonances that hybridizes with the guided mode inside the dielectric layer. The calculated reflection phase difference between the 0th order reflected and incident electric field, as shown in Fig. 13 (a) for normal incidence (red line), and 2^o incidence (blue line), clearly shows that the resonances are magnetic in nature when the surface resonances intersect the zone center at Γ_2 (13.2THz) and Γ_4 (54.3THz) as the reflection phase is zero like what a magnetic conductor surface does to the incident waves. The state Γ_3, invisible in the reflection phase spectrum under normal incidence [red solid line in Fig. 13 (a)], is a dark state as its eigenmode is in mirror symmetry about the yz plane and can not couple with free space photons. While the other B_3 states can couple with external light under oblique incidence [see the blue line in Fig. 13 (a)]. For example, there exists in-phase reflection at frequency 50.22THz under an incident angle of 2o, corresponding a B_3 state at frequency 50.22THz and $k_{0_{\parallel}} \approx 0.02\pi / p$.

The angle-independent absorption peak at 13.2THz is due to the B_2 mode, which is only weakly dispersive near the zone center. The more dispersive B_3 and B_4 modes are accountable for the incident-angle sensitive absorption in the higher frequencies in Fig. 12 (a). The field patterns in Figs. 14 (a)-14 (c) present the spatial distribution of the real part of magnetic fields excited by the incident plane waves with incident angles 0^o, 2^o and 0^o for the three surface resonance states on B_2, B_3 and B_4 respectively, and the corresponding vector diagrams of electric fields are shown in Figs 14 (d)-14 (f). We can see clearly that the electric fields reach maximum in strength at the slab upper surface, and exponentially decay along the surface normal into the free space. This is precisely a picture of SPP modes. The field patterns comes from the coincidence of the evanescent wave components in high Bloch orders at both sides of metallic grating.

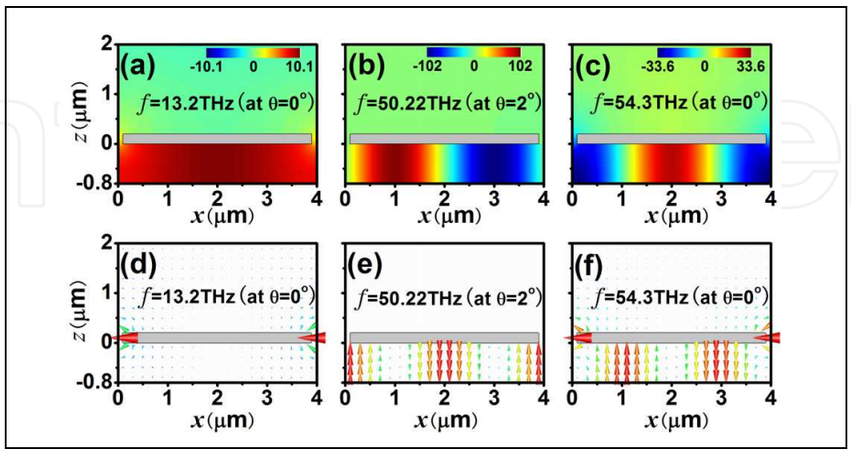

Fig. 14. Spatial distributions of magnetic fields and electric fields in the xz plane for Γ_2 state at f_{Γ_2} =13.2THz, $\theta = 0^o$ [(a) and (c)], a state on B_3 at f=50.22THz, $\theta = 2^o$ [(b) and (e)]and Γ_4 state at f_{Γ_4} =54.3THz, $\theta = 0^o$ [(c) and (f)]

Although only TEM guided modes are allowed to be excited in the thin MDM slab within the frequency of our interest, the B_2 states are quite different from the B_3 and B_4 states in field patterns inside the dielectric layer. We see from Figs. 14 (b), 14 (c) ,14 (e)and 14 (f) that for a B_3 or B_4 state, there are nodes and anti-nodes in field patterns, while for the B_2 state, the magnetic field is almost uniformly distributed. Calculations on local field enhancement inside the dielectric slab resolve the puzzle. Black solid line in Fig. 15 presents the normalized magnetic field $|H|$ inside the dielectric with respect to that of incidence $|H_0|$ under an incident angle of $\theta = 2^o$. The Fourier component in *m=0* order [blue solid line] contributes the most at 13.2THz and the least at 50.22THz and 54.3THz; while it is just opposite for the contributions in combination from the two high order Fourier components with *m=±1* [red solid line]. Figure 15 also indicates that the enhancement of local field of an excited B_3 or B_4 state can be ten times larger than that of an excited B_2 state, the enhancement factor at 50.22THz is about 100 times, while it is only 10 times at 13.2THz.

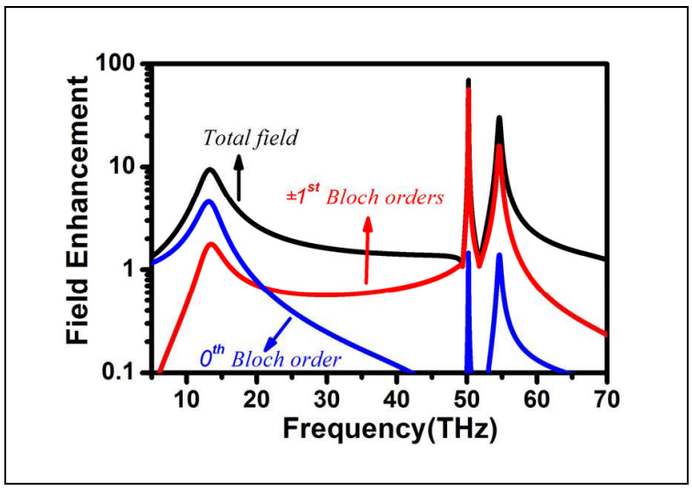

Fig. 15. Magnetic field H inside the dielectric layer normalized to that of incidence H under an incident angle of $\theta = 2^o$. Black line: all Bloch orders of TEM guided modes included; Red line: only the 0th Bloch order considered; Blue line: summation of -1st and +1st Bloch orders of TEM guided modes.

We see from Fig. 13 (b) that the surface resonance dispersion of the slab comes from the interaction between the magnetic resonances and the (folded) light lines L_1 (for dielectrics) and L_2 (for air) grazing on the interfaces. In the limit of a small gap-period ratio ($g/p = 0.05$ for example), our system is weakly Bragg-scattered, and as such, when a surface resonance state on branches B_3 or B_4 is excited, the induced wave fields inside the dielectric of region III are guided quasi-TEM modes dominated by $\pm 1^{st}$ Bloch orders. For that reason, the B_3 and B_4 states have high fidelity even though they are leaky modes, as most of their Bloch wavefunction components lying outside the free space light line. As the air gaps of the metallic grating serve to couple the electromagnetic waves of region I and region III, the quality factor of a resonance state can be estimated with the overlap integral between the fundamental waveguide mode $|\alpha_0>$ in the air gap and the dominant Bloch waves $|\vec{k}_m^i>$ ($i = I, III$) in region I or region III for the coupling coefficients

$$C_m^i = \frac{1}{w_x}\int_0^p \frac{k_{zm}^i}{\sqrt{\varepsilon_r}\sqrt{k_x^{\,2}+k_{zm}^{i\,2}}} e^{-i(k_x+G_m)x} g_0(x)dx$$
$$= \frac{1}{\sqrt{\varepsilon_r}} \frac{k_{zm}^i}{\sqrt{k_x^{\,2}+k_{zm}^{i\,2}}} \sin c[\frac{(k_x+G_m)g}{2}], \quad (13)$$

when the air gap width $g \ll p$ is satisfied. For the B_2 states, the major Fourier component of the wavefunction is $|\vec{k}_0^{\,i}>$ in zero order, and as k_{z0}^{III} is generally not small, C_0^{III} is usually very large according to Eq. 3, and the B_2 states leak out easily. The states on branches B_3 and B_4 have major Fourier components in m=±1 order, and as they are asymptotic to the (folded) dielectric light lines L1, the absolute value of k_{zm}^{III} ($m=+1$ for $k_x<0$ or $m=-1$ for $k_x>0$) is very small, resulting in the small coupling coefficients C_{-1}^{III} or C_{+1}^{III}. The B_3 and B_4 modes have to travel a long distance before they leak out. They have a long life time and a good spatial coherence. It also explains why the state Γ_3, a state precisely superposing on folded light line L'_1 in dielectric layer, is dark to the incident plane wave as $k_{zm}^{III}=0$.

Different from B_3 and B_4 states, the B_2 states have a major Fourier component in m=0 order which directly couples to the free space photons. As a consequence, the B_2 states, forming a flat band far away from the light line L_2 when $\vec{k}_{0_{\parallel}}$ is small, are localized with resonant frequency scaled by local geometry of unit cell. The high mode fidelity of a B_3 or B_4 state also gives rise to much more intense local field compared to the B_2 states. As shown in Fig. 15, the induced local field is 100 times stronger than the incident field for the state on B_3; while it is only 10 times stronger for Γ_2, and this is consistent with the absorptivity shown in Fig. 12 (a). In addition, the coherent length can be adjusted by the gap width as the kernel $\langle\alpha_0|\vec{r}|k_m^i\rangle$ is proportional to the gap-period ratio g/p. More calculations demonstrate that the angular FWHM of the absorption peak is reduced from 0.26^o to 0.16^o when the gap is decreased from $0.2\mu m$ to $0.1\mu m$, corresponding to a coherent length of 358λ.

We note that most of the attentions in previous studies have been devoted on the localized B_2 states (Hibbins, Sambles et al. 2004; Hibbins, Murray et al. 2006; Brown, Hibbins et al. 2008; Diem, Koschny et al. 2009). While the spatially coherent surface resonance states will lead us into a new vision about coherent control of emission radiations. J.-J. Greffet and co-workers showed that highly directional and spatially coherent thermal emission can be obtained by etching a periodic grating structure into a SiC surface (Le Gall, Olivier et al. 1997; Carminati & Greffet 1999; Greffet, Carminati et al. 2002; Marquier, Joulain et al. 2004). The magnetic resonant modes in our system can do the same, as will be demonstrated below. Our system has the advantage that the operational frequency is tunable by changing the structural parameters, and the operational bandwidth is wide. In addition, our structure supports all-angle functionality for some specific range of frequencies as shown in Fig. 16, although it is periodic only in one direction.

We performed finite-difference-in-time-domain (FDTD) simulations to emulate the emissions from a slab containing point sources with random phases using the same configuration parameters aforementioned. We purposely put disorder in structure to test the robustness of the phenomena. We assigned two Gaussian distributions (they can be uniform

distributions or other types as well) independently to the width of metallic strips and the center positions of air gaps to introduce a 4% (standard deviation) structural disorder. The slab has a lateral size of 60 periods along the $\hat{x}$ direction. A total of 1200 point sources with random phases are placed at the mesh points inside the dielectric layer. Directional emissions of a wide range of frequencies above 34THz are confirmed by the simulation. The 4% structural disorder has little impact on the directional emissivity. Fig. 16 (a), 16 (c) and 16 (e) show the far-field emission patterns in the $\hat{x}\hat{z}$ plane (H-plane) at 40.0THz, 54.3THz and 58.0THz. The inset in Fig. 16 (c) is a control calculation in which the top metal gratings are removed, so that there is just a dielectric layer with random phase sources above a metal ground plane. The directivity of emission from the random sources is lost. Fig. 16 (b), 16 (d) and 16 (e) present the absorptivity (under plane wave incidence) as a function of in-plane wave-vector (solid angle) at these frequencies. The strong angle selectivity of the absorption is evident, and by Kirchhoff's law, the thermal emission should also be highly directional, which is a direct consequence of the good spatial coherence of the surface resonance states. As shown in Figs. 16 (b), 16 (d) and 16 (f), the absorption/emission peaks generally trace out an arc in the k_x-k_y plane, but near $54.3THz$ [Fig. 16 (d)], the dominant emission beam is restricted to a small region near the zone center. This is because the Γ_4 state is a minimum point if we consider the band structure in the k_x-k_y plane. That means that at $54.3THz$, we can obtain a directional emission beam not just in the H-plane, but in all directions, although the structure is periodic in only one direction.

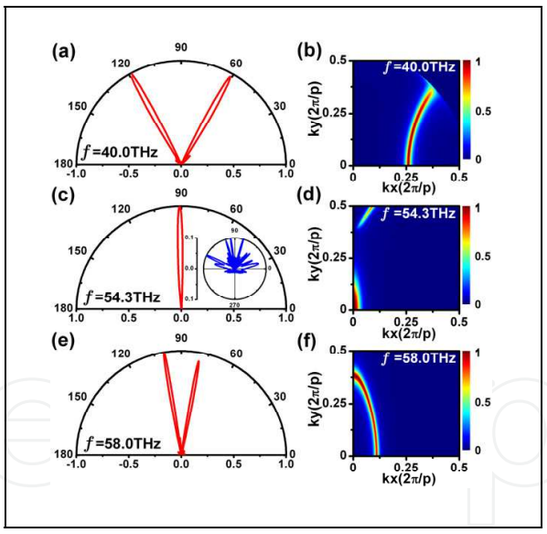

Fig. 16. Radiation patterns in the H-plane (calculated by FDTD) and absorptivity (calculated by mode expansion method) as a function of in-plane wavevectors at f=40.0THz[(a) and (b)], f=54.3THz[(c) and (d)] and f=58.0THz[(e) and (f)]. In FDTD simulations, 1200 point sources with random phases are placed at the mesh points inside the dielectric layer. A 4% structural disorder is included in the80μmsimulation cell, which accounts for the slight asymmetry of the radiation patterns, but also demonstrates the robustness of the angle selectivity with respect to disorder.The inset in (c) is a control calculation in which the top metal gratings are removed, so that there is just a dielectric layer with random phase sources above a metal ground plane. The directivity of emission from the random sources is lost.

We note that there are other schemes to realize coherent thermal radiations, such as by utilizing three-dimensional photonic crystals (Laroche, Carminati et al. 2006) or one-dimensional photonic crystal cavities (Lee, Fu et al. 2005). Our metamaterial slab presents a route to achieve linearly polarized coherent thermal emission radiations in a wide frequency range which can be tuned by adjusting structural parameters and material parameters.

In summary, we proposed a simple metamaterial slab structure that possesses spatially coherent magnetic surface resonance states in a broad range of frequencies. These states facilitate nearly perfect absorption in a thin metamaterial slab containing slightly absorptive materials. As the absorption spectrum is very narrow and sensitive to incident angle, the slab should support directional thermal emission. Direct FDTD simulation with random-phase sources corroborates the existence of strong angular emissivity even in the presence of structural disorder. As the surface resonances originate from artificial resonators, the operational frequency and the response can be tuned by varying the structural configurations. Our findings constitute a simple solution for coherent control of thermal emissions, optical antennas, infrared or THz spectroscopy as well as photon detector.

3. Conclusion

We have shown that a strategy of stacking a multiple layers of holey metallic slabs can give rise to wide transparency band. The multi-layered structure, well known as fishnet metamaterial, also supports broadband negative refraction and sub-wavelength imaging provided that the light waves are incident on its sidewall interface. We also show that coherent control of spontaneous emission radiations can be realizing in a wide frequency range by utilizing spatially coherent magnetic surface resonance states of a magnetic meta-surface. The modal expansion method, developed for magnetic meta-surface and multi-layered holey metallic slabs, is very fruitful for semi-analytical interpretation on the behind physics picture of planar metamaterials.

4. Acknowledgment

H. Li thanks Prof. C.T. Chan, Prof. H. Chen and Prof. D. Z. Zhang for the collaboration and helpful discussion. This work was supported by NSFC (No. 11174221, 10974144, 60678046, 10574099), CNKBRSF (Grant No. 2011CB922001), the National 863 Program of China (No.2006AA03Z407), NCET (07-0621), STCSM and SHEDF (No. 06SG24).

5. References

Andrew, P.; Kitson, S. C. & Barnes, W. L. (1997). Surface-plasmon energy gaps and photoabsorption. *Journal of Modern Optics* Vol. 44 No. 2, (FEB 1997) pp. 395-406,ISSN 0950-0340

Bahk, Y. M.; Park, H. R.; Ahn, K. J.; Kim, H. S.; Ahn, Y. H.; Kim, D. S.; Bravo-Abad, J.; Martin-Moreno, L. & Garcia-Vidal, F. J. (2011). Anomalous Band Formation in Arrays of Terahertz Nanoresonators. *Physical Review Letters* Vol. 106 No. 1, (Jan 5) pp. 013902-013904,ISSN 0031-9007

Baida, F. I.; Van Labeke, D.; Granet, G.; Moreau, A. & Belkhir, A. (2004). Origin of the super-enhanced light transmission through a 2-D metallic annular aperture array: a study of photonic bands. *Applied Physics B: Lasers and Optics* Vol. 79 No. 1, (JUL 2004) pp. 1-8,ISSN 0946-2171

Barnes, W. L.; Dereux, A. & Ebbesen, T. W. (2003). Surface plasmon subwavelength optics. *Nature* Vol. 424 No. 6950, (Aug 14) pp. 824-830,ISSN 0028-0836

Belov, P.; Hao, Y. & Sudhakaran, S. (2006). Subwavelength microwave imaging using an array of parallel conducting wires as a lens. *Physical Review B* Vol. 73 No. JAN 2006) pp. 033108-033104,ISSN 1098-0121

Beruete, M.; Campillo, I.; Rodriguez-Seco, J. E.; Perea, E.; Navarro-Cia, M.; Nunez-Manrique, I. J. & Sorolla, M. (2007). Enhanced gain by double-periodic stacked subwavelength hole array. *Ieee Microwave and Wireless Components Letters* Vol. 17 No. 12, (Dec) pp. 831-833,ISSN 1531-1309

Beruete, M.; Navarro-Cia, M.; Sorolla, M. & Campillo, I. (2008). Polarization selection with stacked hole array metamaterial. *Journal of Applied Physics* Vol. 103 No. 5, (Mar) pp. 053102-053104,ISSN 0021-8979

Beruete, M.; Sorolla, M.; Navarro-Cia, M.; Falcone, F.; Campillo, I. & Lomakin, V. (2007). Extraordinary transmission and left-handed propagation in miniaturized stacks of doubly periodic subwavelength hole arrays. *Optics Express* Vol. 15 No. 3, (Feb) pp. 1107-1114,ISSN 1094-4087

Boltasseva, A. & Shalaev, V. M. (2008). Fabrication of optical negative-index metamaterials: Recent advances and outlook. *Metamaterials* Vol. 2 No. 1, (pp. 1-17,ISSN 1873-1988

Born, M. & Wolf, E. (1980). Principles of Optics: Electromagnetic Theory of Propagation, Interference and Diffraction of Light. Oxford, Angleterre, Pergamon Press.

Brown, J.; Hibbins, A.; Lockyear, M.; Lawrence, C. & Sambles, J. (2008). Angle-independent microwave absorption by ultrathin microcavity arrays. *Journal of Applied Physics* Vol. 104 No. 4, (AUG 15 2008) pp. 043105,ISSN 0021-8979

Cao, J. X.; Liu, H.; Li, T.; Wang, S. M.; Li, T. Q.; Zhu, S. N. & Zhang, X. (2009). Steering polarization of infrared light through hybridization effect in a tri-rod structure. *Journal of the Optical Society of America B-Optical Physics* Vol. 26 No. 12, (Dec) pp. B96-B101,ISSN 0740-3224

Cao, R.; Wei Z.Y.; Li W.; Fang, A.A. Li, H.Q.; Jiang, X.Y.; Chen, H. & Chan, C.T. (2011). Low-threshold directional plasmon lasing assisted by spatially coherent surface plasmon polaritons. *arXiv:1106.3002v1*

Carminati, R. & Greffet, J.-J. (1999). Near-field effects in spatial coherence of thermal sources. *Physical Review Letters* Vol. 82 No. 8, (FEB 22 1999) pp. 1660-1663,ISSN 0031-9007

Chan, H. B.; Marcet, Z.; Woo, K.; Tanner, D. B.; Carr, D. W.; Bower, J. E.; Cirelli, R. A.; Ferry, E.; Klemens, F.; Miner, J.; Pai, C. S. & Taylor, J. A. (2006). Optical transmission through double-layer metallic subwavelength slit arrays. *Optics Letters* Vol. 31 No. 4, (Feb 15) pp. 516-518,ISSN 0146-9592

Chin, J. Y.; Gollub, J. N.; Mock, J. J.; Liu, R. P.; Harrison, C.; Smith, D. R. & Cui, T. J. (2009). An efficient broadband metamaterial wave retarder. *Optics Express* Vol. 17 No. 9, (Apr 27) pp. 7640-7647,ISSN 1094-4087

Chin, J. Y.; Lu, M. Z. & Cui, T. J. (2008). Metamaterial polarizers by electric-field-coupled resonators. *Applied Physics Letters* Vol. 93 No. 25, (Dec 22) pp. 251903,ISSN 0003-6951

Coutaz, J. L.; Neviere, M.; Pic, E. & Reinisch, R. (1985). Experimental study of surface-enhanced second-harmonic generation on silver gratings. *Physical Review B* Vol. 32 No. 4,pp. 2227-2232

de Abajo, F. J. G. & Saenz, J. J. (2005). Electromagnetic surface modes in structured perfect-conductor surfaces. *Physical Review Letters* Vol. 95 No. 23, (Dec 2) pp. 233901-233904,ISSN 0031-9007

Diem, M.; Koschny, T. & Soukoulis, C. (2009). Wide-angle perfect absorber/thermal emitter in the terahertz regime. *Physical Review B* Vol. 79 No. 3, (JAN 2009) pp. 033101,ISSN 1098-0121

Dolling, G.; Enkrich, C.; Wegener, M.; Soukoulis, C. & Linden, S. (2006). Simultaneous negative phase and group velocity of light in a metamaterial. *Science* Vol. 312 (MAY 12 2006) pp. 892-894,ISSN 0036-8075

Dolling, G.; Wegener, M. & Linden, S. (2007). Realization of a three-functional-layer negative-index photonic metamaterial. *Optics Letters* Vol. 32 No. 5, (Mar) pp. 551-553,ISSN 0146-9592

Ebbesen, T. W.; Lezec, H. J.; Ghaemi, H. F.; Thio, T. & Wolff, P. A. (1998). Extraordinary optical transmission through sub-wavelength hole arrays. *Nature* Vol. 391 No. 6668, (FEB 12 1998) pp. 667-669,ISSN 0028-0836

Eisenberg, H.; Silberberg, Y.; Morandotti, R. & Aitchison, J. (2000). Diffraction management. *Physical Review Letters* No. AUG 28 2000) pp. 1863-1866,ISSN 0031-9007

Engheta, N. & Ziolkowski, R. W. (2006). *Metamaterials: physics and engineering explorations*, Wiley & Sons.

Fan, W. J.; Zhang, S.; Malloy, K. J. & Brueck, S. R. J. (2005). Enhanced mid-infrared transmission through nanoscale metallic coaxial-aperture arrays. *Optics Express* Vol. 13 No. 12, (JUN 13 2005) pp. 4406-4413,ISSN 1094-4087

Fan, W. J.; Zhang, S.; Minhas, B.; Malloy, K. J. & Brueck, S. R. J. (2005). Enhanced infrared transmission through subwavelength coaxial metallic arrays. *Physical Review Letters* Vol. 94 No. 3, (JAN 28 2005) pp. 033902,ISSN 0031-9007

Fan, X.; Wang, G.; Lee, J. & Chan, C. T. (2006). All-angle broadband negative refraction of metal waveguide arrays in the visible range: Theoretical analysis and numerical demonstration. *Physical Review Letters* Vol. 97 No. AUG 18 2006) pp. 073901-073904,ISSN 0031-9007

Fan, Y. C.; Han, J.; Wei, Z. Y.; Wu, C.; Cao, Y.; Yu, X. & Li, H. Q. (2011). Subwavelength electromagnetic diode: One-way response of cascading nonlinear meta-atoms. *Applied Physics Letters* Vol. 98 No. 15, (Apr 11) pp. 151903,ISSN 0003-6951

Fedotov, V. A.; Schwanecke, A. S.; Zheludev, N. I.; Khardikov, V. V. & Prosvirnin, S. L. (2007). Asymmetric transmission of light and enantiomerically sensitive plasmon resonance in planar chiral nanostructures. *Nano Letters* Vol. 7 No. 7, (Jul) pp. 1996-1999,ISSN 1530-6984

Freire, M.; Marques, R. & Jelinek, L. (2008). Experimental demonstration of a mu=-1 metamaterial lens for magnetic resonance imaging. *Applied Physics Letters* Vol. 93 No. DEC 8 2008) pp. 231108-231101,ISSN 0003-6951

Gay, G.; Alloschery, O.; de Lesegno, B. V.; Weiner, J. & Lezec, H. J. (2006). Surface wave generation and propagation on metallic subwavelength structures measured by far-field interferometry. *Physical Review Letters* Vol. 96 No. 21, (Jun 2) pp. 213901-213904,ISSN 0031-9007

Ghaemi, H. F.; Thio, T.; Grupp, D. E.; Ebbesen, T. W. & Lezec, H. J. (1998). Surface plasmons enhance optical transmission through subwavelength holes. *Physical Review B* Vol. 58 No. 11, (SEP 15 1998) pp. 6779-6782,ISSN 1098-0121

Grbic, A. & Eleftheriades, G. (2004). Overcoming the diffraction limit with a planar left-handed transmission-line lens. *Physical Review Letters* Vol. 92 (MAR 19 2004) pp. 117403-117404,ISSN 0031-9007

Greffet, J.-J.; Carminati, R.; Joulain, K.; Mulet, J.-P.; Mainguy, S. & Chen, Y. (2002). Coherent emission of light by thermal sources. *Nature* Vol. 416 No. 6876, (Mar 7) pp. 61-64,ISSN 0028-0836

Greffet, J.-J. & Nieto-Vesperinas, M. (1998). Field theory for generalized bidirectional reflectivity: derivation of Helmholtz's reciprocity principle and Kirchhoff's law. *Journal of the Optical Society of America A* Vol. 15 No. 10 pp. 2735-2744

Grigorenko, A. N.; Geim, A. K.; Gleeson, H. F.; Zhang, Y.; Firsov, A. A.; Khrushchev, I. Y. & Petrovic, J. (2005). Nanofabricated media with negative permeability at visible frequencies. *Nature* Vol. 438 No. 7066, (NOV 17 2005) pp. 335-338,ISSN 0028-0836

Han, J.; Li, H. Q.; Fan, Y. C.; Wei, Z. Y.; Wu, C.; Cao, Y.; Yu, X.; Li, F. & Wang, Z. S. (2011). An ultrathin twist-structure polarization transformer based on fish-scale metallic wires. *Applied Physics Letters* Vol. 98 No. 15, (Apr 11) pp. 151908,ISSN 0003-6951

Hao, J. M.; Yuan, Y.; Ran, L. X.; Jiang, T.; Kong, J. A.; Chan, C. T. & Zhou, L. (2007). Manipulating electromagnetic wave polarizations by anisotropic metamaterials. *Physical Review Letters* Vol. 99 No. 6, (Aug 10) pp. 063908,ISSN 0031-9007

Haus, H. & Molter-Orr, L. (1983). Coupled multiple waveguide systems. *Quantum Electronics, IEEE Journal of* Vol. 19 No. 5, (pp. 840-844,ISSN 0018-9197

Hibbins, A.; Murray, W.; Tyler, J.; Wedge, S.; Barnes, W. & Sambles, J. (2006). Resonant absorption of electromagnetic fields by surface plasmons buried in a multilayered plasmonic nanostructure. *Physical Review B* Vol. 74 No. 7, (AUG 2006) pp. 073408,ISSN 1098-0121

Hibbins, A.; Sambles, J.; Lawrence, C. & Brown, J. (2004). Squeezing millimeter waves into microns. *Physical Review Letters* Vol. 92 No. 14, (APR 9 2004) pp. 143904,ISSN 0031-9007

Hibbins, A. P.; Evans, B. R. & Sambles, J. R. (2005). Experimental verification of designer surface plasmons. *Science* Vol. 308 No. 5722, (APR 29 2005) pp. 670-672,ISSN 0036-8075

Kamli, A.; Moiseev, S. A. & Sanders, B. C. (2008). Coherent Control of Low Loss Surface Polaritons. *Physical Review Letters* Vol. 101 No. 26, (DEC 31 2008) pp. 263601,ISSN 0031-9007

Kneipp, K.; Wang, Y.; Kneipp, H.; Perelman, L. T.; Itzkan, I.; Dasari, R. R. & Feld, M. S. (1997). Single molecule detection using surface-enhanced Raman scattering (SERS). *Physical Review Letters* Vol. 78 No. 9, (MAR 3 1997) pp. 1667-1670,ISSN 0031-9007

Ku, Z. & Brueck, S. R. J. (2009). Experimental demonstration of sidewall angle induced bianisotropy in multiple layer negative index metamaterials. *Applied Physics Letters* Vol. 94 No. 15, (Apr) pp. 153107-153103,ISSN 0003-6951

Ku, Z. Y.; Zhang, J. Y. & Brueck, S. R. J. (2009). Bi-anisotropy of multiple-layer fishnet negative-index metamaterials due to angled sidewalls. *Optics Express* Vol. 17 No. 8, (Apr) pp. 6782-6789,ISSN 1094-4087

Lalanne, P.; Hugonin, J. P.; Astilean, S.; Palamaru, M. & Moller, K. D. (2000). One-mode model and Airy-like formulae for one-dimensional metallic gratings. *Journal of Optics a-Pure and Applied Optics* Vol. 2 No. 1, (Jan) pp. 48-51,ISSN 1464-4258

Laroche, M.; Carminati, R. & Greffet, J.-J. (2006). Coherent thermal antenna using a photonic crystal slab. *Physical Review Letters* Vol. 96 No. 12, (MAR 31 2006) pp. 123903,ISSN 0031-9007

Le Gall, J.; Olivier, M. & Greffet, J.-J. (1997). Experimental and theoretical study of reflection and coherent thermal emission by a SiC grating supporting a surface-phonon polariton. *Physical Review B* Vol. 55 No. 15, (APR 15 1997) pp. 10105-10114,ISSN 0163-1829

Lee, B. J.; Fu, C. J. & Zhang, Z. M. (2005). Coherent thermal emission from one-dimensional photonic crystals. *Applied Physics Letters* Vol. 87 No. 7, (Aug) pp. 071904,ISSN 0003-6951

Li, H. Q.; Hang, Z. H.; Qin, Y. Q.; Wei, Z. Y.; Zhou, L.; Zhang, Y. W.; Chen, H. & Chan, C. T. (2005). Quasi-periodic planar metamaterial substrates. *Applied Physics Letters* Vol. 86 No. 12, (MAR 21 2005) pp. 121108,ISSN 0003-6951

Li, H. Q.; Hao, J. M.; Zhou, L.; Wei, Z. Y.; Gong, L. K.; Chen, H. & Chan, C. T. (2006). All-dimensional subwavelength cavities made with metamaterials. *Applied Physics Letters* Vol. 89 No. 10, (SEP 4 2006) pp. 104101-104103,ISSN 0003-6951

Li, T.; Liu, H.; Wang, S. M.; Yin, X. G.; Wang, F. M.; Zhu, S. N. & Zhang, X. A. (2008). Manipulating optical rotation in extraordinary transmission by hybrid plasmonic excitations. *Applied Physics Letters* Vol. 93 No. 2, (Jul 14) pp. 021110,ISSN 0003-6951

Li, T. Q.; Liu, H.; Li, T.; Wang, S. M.; Wang, F. M.; Wu, R. X.; Chen, P.; Zhu, S. N. & Zhang, X. (2008). Magnetic resonance hybridization and optical activity of microwaves in a chiral metamaterial. *Applied Physics Letters* Vol. 92 No. 13, (Mar 31) pp. 131111,ISSN 0003-6951

Liu, H.; Genov, D.; Wu, D.; Liu, Y.; Steele, J.; Sun, C.; Zhu, S. & Zhang, X. (2006). Magnetic plasmon propagation along a chain of connected subwavelength resonators at infrared frequencies. *Physical Review Letters* Vol. 97 No. 24, (DEC 15 2006) pp. 243902,ISSN 0031-9007

Liu, H.; Genov, D. A.; Wu, D. M.; Liu, Y. M.; Liu, Z. W.; Sun, C.; Zhu, S. N. & Zhang, X. (2007). Magnetic plasmon hybridization and optical activity at optical frequencies in metallic nanostructures. *Physical Review B* Vol. 76 No. 7, (Aug) pp. 073101,ISSN 1098-0121

Liu, H. T. & Lalanne, P. (2008). Microscopic theory of the extraordinary optical transmission. *Nature* Vol. 452 No. 7188, (Apr 10) pp. 728-731,ISSN 0028-0836

Liu, N.; Guo, H. C.; Fu, L. W.; Kaiser, S.; Schweizer, H. & Giessen, H. (2008). Three-dimensional photonic metamaterials at optical frequencies. *Nature Materials* Vol. 7 No. 1, (Jan) pp. 31-37,ISSN 1476-1122

Lockyear, M. J.; Hibbins, A. P. & Sambles, J. R. (2009). Microwave Surface-Plasmon-Like Modes on Thin Metamaterials. *Physical Review Letters* Vol. 102 No. 7, (FEB 20 2009) pp. 073901,ISSN 0031-9007

Mansuripur, M. (2002). Classical Optics and its Applications, Cambridge University Press.

Marcet, Z.; Hang, Z. H.; Chan, C. T.; Kravchenko, I.; Bower, J. E.; Cirelli, R. A.; Klemens, F.; Mansfield, W. M.; Miner, J. F.; Pai, C. S. & Chan, H. B. (2010). Optical transmission through double-layer, laterally shifted metallic subwavelength hole arrays. *Optics Letters* Vol. 35 No. 13, (Jul 1) pp. 2124-2126,ISSN 0146-9592

Marquier, F.; Joulain, K.; Mulet, J.-P.; Carminati, R.; Greffet, J.-J. & Chen, Y. (2004). Coherent spontaneous emission of light by thermal sources. *Physical Review B* Vol. 69 No. 15, (APR 2004) pp. 155412,ISSN 1098-0121

Martin-Moreno, L.; Garcia-Vidal, F. J.; Lezec, H. J.; Pellerin, K. M.; Thio, T.; Pendry, J. B. & Ebbesen, T. W. (2001). Theory of extraordinary optical transmission through subwavelength hole arrays. *Physical Review Letters* Vol. 86 No. 6, (FEB 5 2001) pp. 1114-1117,ISSN 0031-9007

Maystre, D. (2001). Photonic crystal diffraction gratings. *Optics Express* Vol. 8 No. 3, (JAN 29 2001) pp. 209-216,ISSN 1094-4087

Menzel, C.; Helgert, C.; Rockstuhl, C.; Kley, E. B.; Tunnermann, A.; Pertsch, T. & Lederer, F. (2010). Asymmetric Transmission of Linearly Polarized Light at Optical Metamaterials. *Physical Review Letters* Vol. 104 No. 25, (Jun 22) pp. 253902,ISSN 0031-9007

Miyamaru, F. & Hangyo, M. (2005). Anomalous terahertz transmission through double-layer metal hole arrays by coupling of surface plasmon polaritons. *Physical Review B* Vol. 71 No. 16, (Apr) pp. 165408-165405,ISSN 1098-0121

Mocella, V.; Dardano, P.; Moretti, L. & Rendina, I. (2007). Influence of surface termination on negative reflection by photonic crystals. *Optics Express* Vol. 15 No. 11, (MAY 28 2007) pp. 6605-6611,ISSN 1094-4087

Navarro-Cia, M.; Beruete, M.; Sorolla, M. & Campillo, I. (2008). Negative refraction in a prism made of stacked subwavelength hole arrays. *Optics Express* Vol. 16 No. 2, (Jan) pp. 560-566,ISSN 1094-4087

Navarro-Cia, M.; Beruete, M.; Sorolla, M. & Campillo, I. (2009). Converging biconcave metallic lens by double-negative extraordinary transmission metamaterial. *Applied Physics Letters* Vol. 94 No. 14, (Apr) pp. 144107-144103,ISSN 0003-6951

Nie, S. & Emory, S. R. (1997). Probing single molecules and single nanoparticles by surface-enhanced Raman scattering. *Science* Vol. 275 No. 5303, (FEB 21 1997) pp. 1102-1106,ISSN 0036-8075

Ortuno, R.; Garcia-Meca, C.; Rodriguez-Fortuno, F. J.; Marti, J. & Martinez, A. (2009). Role of surface plasmon polaritons on optical transmission through double layer metallic hole arrays. *Physical Review B* Vol. 79 No. 7, (Feb) pp. 075425-075427,ISSN 1098-0121

Pendry, J. B. (2000). Negative refraction makes a perfect lens. *Physical Review Letters* Vol. 85 No. 18, (Oct 30) pp. 3966-3969,ISSN 0031-9007

Pendry, J. B.; Holden, A. J.; Robbins, D. J. & Stewart, W. J. (1999). Magnetism from conductors and enhanced nonlinear phenomena. *Ieee Transactions on Microwave Theory and Techniques* Vol. 47 No. 11, (Nov) pp. 2075-2084,ISSN 0018-9480

Pendry, J. B.; Holden, A. J.; Stewart, W. J. & Youngs, I. (1996). Extremely low frequency plasmons in metallic mesostructures. *Physical Review Letters* Vol. 76 No. 25, (Jun 17) pp. 4773-4776,ISSN 0031-9007

Pendry, J. B.; Martin-Moreno, L. & Garcia-Vidal, F. J. (2004). Mimicking surface plasmons with structured surfaces. *Science* Vol. 305 No. 5685, (Aug 6) pp. 847-848,ISSN 0036-8075

Pertsch, T.; Zentgraf, T.; Peschel, U.; Brauer, A. & Lederer, F. (2002). Anomalous refraction and diffraction in discrete optical systems. *Physical Review Letters* Vol. 88 (MAR 4 2002) pp. 093901-093904,ISSN 0031-9007

Plum, E.; Fedotov, V. A.; Schwanecke, A. S.; Zheludev, N. I. & Chen, Y. (2007). Giant optical gyrotropy due to electromagnetic coupling. *Applied Physics Letters* Vol. 90 No. 22, (May 28) pp. 223113,ISSN 0003-6951

Plum, E.; Zhou, J.; Dong, J.; Fedotov, V. A.; Koschny, T.; Soukoulis, C. M. & Zheludev, N. I. (2009). Metamaterial with negative index due to chirality. *Physical Review B* Vol. 79 No. 3, (Jan) pp. 121104 (R),ISSN 1098-0121

Raether, H. (1988). Surface Plasmons on Smooth and Rough Surfaces and on Gratings. Berlin, Springer-Verlag.

Rayleigh (1907). *Proc. R. Soc. London, Ser. A* Vol. 79 No. pp. 399

Rogacheva, A. V.; Fedotov, V. A.; Schwanecke, A. S. & Zheludev, N. I. (2006). Giant gyrotropy due to electromagnetic-field coupling in a bilayered chiral structure. *Physical Review Letters* Vol. 97 No. 17, (Oct 27) pp. 177401,ISSN 0031-9007

Ruan, Z. C. & Qiu, M. (2006). Enhanced transmission through periodic arrays of subwavelength holes: The role of localized waveguide resonances. *Physical Review Letters* Vol. 96 No. 23, (JUN 16 2006) pp. 233901,ISSN 0031-9007

Shalaev, V. M. (2007). Optical negative-index metamaterials. *Nature Photonics* Vol. 1 No. 1, (JAN 2007) pp. 41-48,ISSN 1749-4885

Shelby, R. A.; Smith, D. R. & Schultz, S. (2001). Experimental verification of a negative index of refraction. *Science* Vol. 292 (APR 6 2001) pp. 77-79,ISSN 0036-8075

Sheng, P.; Stepleman, R. S. & Sanda, P. N. (1982). Exact eigenfunctions for square-wave gratings: Application to diffraction and surface-plasmon calculations. *Physical Review B* Vol. 26 No. 6,pp. 2907-2916,ISSN

Sievenpiper, D.; Zhang, L. J.; Broas, R. F. J.; Alexopolous, N. G. & Yablonovitch, E. (1999). High-impedance electromagnetic surfaces with a forbidden frequency band. *Ieee Transactions on Microwave Theory and Techniques* Vol. 47 No. 11, (Nov) pp. 2059-2074,ISSN 0018-9480

Silveirinha, M.; Fernandes, C. & Costa, J. (2008). Superlens made of a metamaterial with extreme effective parameters. *Physical Review B* Vol. 78 (NOV 2008) pp. 195121-195127,ISSN 1098-0121

Silveirinha, M.; Medeiros, C.; Fernandes, C. & Costa, J. (2010). Experimental verification of broadband superlensing using a metamaterial with an extreme index of refraction. *Physical Review B* Vol. 81 No. JAN 2010) pp. 033301-033304,ISSN 1098-0121

Singh, R.; Plum, E.; Menzel, C.; Rockstuhl, C.; Azad, A. K.; Cheville, R. A.; Lederer, F.; Zhang, W. & Zheludev, N. I. (2009). Terahertz metamaterial with asymmetric transmission. *Physical Review B* Vol. 80 No. 15, (Oct) pp. 153104,ISSN 1098-0121

Smith, D. R.; Pendry, J. B. & Wiltshire, M. C. K. (2004). Metamaterials and negative refractive index. *Science* Vol. 305 No. 5685, (Aug 6) pp. 788-792,ISSN 0036-8075

Taflove, A. & Hagness, S. C. (2000). Computational Electrodynamics: The Finite-Difference Time-Domain Method, 2nd ed. Norwood,MA, Artech House.

Tang, Z. H.; Peng, R. W.; Wang, Z.; Wu, X.; Bao, Y. J.; Wang, Q. J.; Zhang, Z. J.; Sun, W. H. & Wang, M. (2007). Coupling of surface plasmons in nanostructured metal/dielectric multilayers with subwavelength hole arrays. *Physical Review B* Vol. 76 No. 19, (Nov) pp. 195405-195408,ISSN 1098-0121

Tsang, T. Y. F. (1996). Surface-plasmon-enhanced third-harmonic generation in thin silver films. *Optics Letters* Vol. 21 No. 4, (FEB 15 1996) pp. 245-247,ISSN 0146-9592

Valentine, J.; Zhang, S.; Zentgraf, T.; Ulin-Avila, E.; Genov, D.; Bartal, G. & Zhang, X. (2008). Three-dimensional optical metamaterial with a negative refractive index. *Nature* Vol. 455 (SEP 18 2008) pp. 376-379,ISSN 0028-0836

van der Molen, K. L.; Klein Koerkamp, K. J.; Enoch, S.; Segerink, F. B.; van Hulst, N. F. & Kuipers, L. (2005). Role of shape and localized resonances in extraordinary transmission through periodic arrays of subwavelength holes: Experiment and theory. *Physical Review B* Vol. 72 No. 4, (JUL 2005) pp. 045421,ISSN 1098-0121

Vasa, P.; Pomraenke, R.; Schwieger, S.; Mazur, Y. I.; Kunets, V.; Srinivasan, P.; Johnson, E.; Kihm, J. E.; Kim, D. S.; Runge, E.; Salamo, G. & Lienau, C. (2008). Coherent exciton-surface-plasmon-polariton interaction in hybrid metal-semiconductor nanostructures. *Physical Review Letters* Vol. 101 No. 11, (SEP 12 2008) pp. 116801,ISSN 0031-9007

Veselago, V. G. (1968). The electrodynamics of substances with simultaneously negative values of ε and μ. *Sov. Phys. Usp.* Vol. 10 No. 4,pp. 509–514

von Freymann, G.; Koch, W.; Meisel, D. C.; Wegener, M.; Diem, M.; Garcia-Martin, A.; Pereira, S.; Busch, K.; Schilling, J.; Wehrspohn, R. B. & Gosele, U. (2003). Diffraction properties of two-dimensional photonic crystals. *Applied Physics Letters* Vol. 83 No. 4, (JUL 28 2003) pp. 614-616,ISSN 0003-6951

Wei, Z. Y.; Cao, Y.; Han, J.; Wu, C.; Fan, Y. C. & Li, H. Q. (2010). Broadband negative refraction in stacked fishnet metamaterial. *Applied Physics Letters* Vol. 97 No. 14, (Oct) pp. 141901,ISSN 0003-6951

Wei, Z. Y.; Cao, Y.;Fan, Y. C.; Yu, X.; & Li, H. Q. (2011). Broadband enhanced transmission through the stacked metallic multi-layers perforated with coaxial annular apertures. *arXiv:1107.4604*

Wei, Z. Y.; Fu, J. X.; Cao, Y.; Wu, C. & Li, H. Q. (2010). The impact of local resonance on the enhanced transmission and dispersion of surface resonances. *Photonics and Nanostructures - Fundamentals and Applications* Vol. 8 No. 2,pp. 94-101

Wei, Z. Y.; Li, H. Q.; Cao, Y.; Wu, C.; Ren, J. Z.; Hang, Z. H.; Chen, H.; Zhang, D. Z. & Chan, C. T. (2010). Spatially coherent surface resonance states derived from magnetic resonances. *New Journal of Physics* Vol. 12 (SEP 15 2010) pp. 093020,ISSN 1367-2630

Wei, Z. Y.; Li, H. Q.; Wu, C.; Cao, Y.; Ren, J. Z.; Hang, Z. H.; Chen, H.; Zhang, D. Z. & Chan, C. T. (2010). Anomalous reflection from hybrid metamaterial slab. *Optics Express* Vol. 18 (JUN 7 2010) pp. 12119-12126,ISSN 1094-4087

Wen, W. J.; Zhou, L.; Hou, B.; Chan, C. T. & Sheng, P. (2005). Resonant transmission of microwaves through subwavelength fractal slits in a metallic plate. *Physical Review B* Vol. 72 No. 15, (Oct) pp. 153406-153404,ISSN 1098-0121

Wiltshire, M.; Pendry, J. & Hajnal, J. (2006). Sub-wavelength imaging at radio frequency. *Journal of Physics-Condensed Matter* Vol. 18 (JUN 7 2006) pp. L315-L321,ISSN 0953-8984

Wood, R. W. (1935). Anomalous Diffraction Gratings. *Physical Review* Vol. 48 No. 12, (pp. 928-936,ISSN

Xiao, X. A.; Jinbo, W.; Sasagawa, Y.; Miyamaru, F.; Zhang, M. Y.; Takeda, M. W.; Qiu, C. Y.; Wen, W. J. & Sheng, P. (2010). Resonant terahertz transmissions through metal hole array on silicon substrate. *Optics Express* Vol. 18 No. 18, (Aug 30) pp. 18558-18564,ISSN 1094-4087

Ye, Y. H. & Zhang, J. Y. (2005). Enhanced light transmission through cascaded metal films perforated with periodic hole arrays. *Optics Letters* Vol. 30 No. 12, (Jun 15) pp. 1521-1523,ISSN 0146-9592

Ye, Y. Q. & He, S. (2010). 90 degrees polarization rotator using a bilayered chiral metamaterial with giant optical activity. *Applied Physics Letters* Vol. 96 No. 20, (May 17) pp. 203501,ISSN 0003-6951

Yen, T. J.; Padilla, W. J.; Fang, N.; Vier, D. C.; Smith, D. R.; Pendry, J. B.; Basov, D. N. & Zhang, X. (2004). Terahertz magnetic response from artificial materials. *Science* Vol. 303 No. 5663, (Mar 5) pp. 1494-1496,ISSN 0036-8075

Zhang, S.; Fan, W.; Panoiu, N.; Malloy, K.; Osgood, R. & Brueck, S. (2006). Optical negative-index bulk metamaterials consisting of 2D perforated metal-dielectric stacks. *Optics Express* Vol. 14 (JUL 24 2006) pp. 6778-6787,ISSN 1094-4087

Zhou, L.; Huang, C. P.; Wu, S.; Yin, X. G.; Wang, Y. M.; Wang, Q. J. & Zhu, Y. Y. (2010). Enhanced optical transmission through metal-dielectric multilayer gratings. *Applied Physics Letters* Vol. 97 No. 1, (Jul 5) pp. 011905-011903,ISSN 0003-6951

Zhou, L.; Li, H. Q.; Qin, Y. Q.; Wei, Z. Y. & Chan, C. T. (2005). Directive emissions from subwavelength metamaterial-based cavities. *Applied Physics Letters* Vol. 86 No. 10, (MAR 7 2005) pp. 101101,ISSN 0003-6951

Zhou, L.; Wen, W.; Chan, C. & Sheng, P. (2003). Multiband subwavelength magnetic reflectors based on fractals. *Applied Physics Letters* Vol. 83 (OCT 20 2003) pp. 3257-3259,ISSN 0003-6951

Zhu, B.; Feng, Y. J.; Zhao, J. M.; Huang, C. & Jiang, T. A. (2010). Switchable metamaterial reflector/absorber for different polarized electromagnetic waves. *Applied Physics Letters* Vol. 97 No. 5, (Aug 2) pp. 051906,ISSN 0003-6951

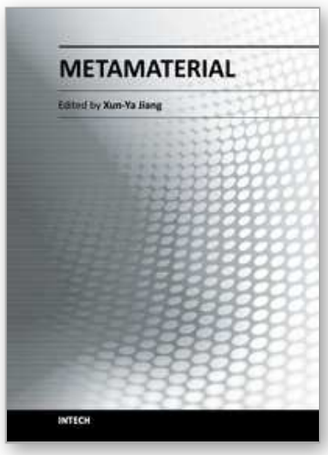

Metamaterial

Edited by Dr. Xun-Ya Jiang

ISBN 978-953-51-0591-6
Hard cover, 620 pages
Publisher InTech
Published online 16, May, 2012
Published in print edition May, 2012

In-depth analysis of the theory, properties and description of the most potential technological applications of metamaterials for the realization of novel devices such as subwavelength lenses, invisibility cloaks, dipole and reflector antennas, high frequency telecommunications, new designs of bandpass filters, absorbers and concentrators of EM waves etc. In order to create a new devices it is necessary to know the main electrodynamical characteristics of metamaterial structures on the basis of which the device is supposed to be created. The electromagnetic wave scattering surfaces built with metamaterials are primarily based on the ability of metamaterials to control the surrounded electromagnetic fields by varying their permeability and permittivity characteristics. The book covers some solutions for microwave wavelength scales as well as exploitation of nanoscale EM wavelength such as visible specter using recent advances of nanotechnology, for instance in the field of nanowires, nanopolymers, carbon nanotubes and graphene. Metamaterial is suitable for scholars from extremely large scientific domain and therefore given to engineers, scientists, graduates and other interested professionals from photonics to nanoscience and from material science to antenna engineering as a comprehensive reference on this artificial materials of tomorrow.

INTECH
open science | open minds

InTech Europe
University Campus STeP Ri
Slavka Krautzeka 83/A
51000 Rijeka, Croatia
Phone: +385 (51) 770 447
Fax: +385 (51) 686 166
www.intechopen.com

InTech China
Unit 405, Office Block, Hotel Equatorial Shanghai
No.65, Yan An Road (West), Shanghai, 200040, China
中国上海市延安西路65号上海国际贵都大饭店办公楼405单元
Phone: +86-21-62489820
Fax: +86-21-62489821

IntechOpen